Abstracta

Ano XXII - N. 03

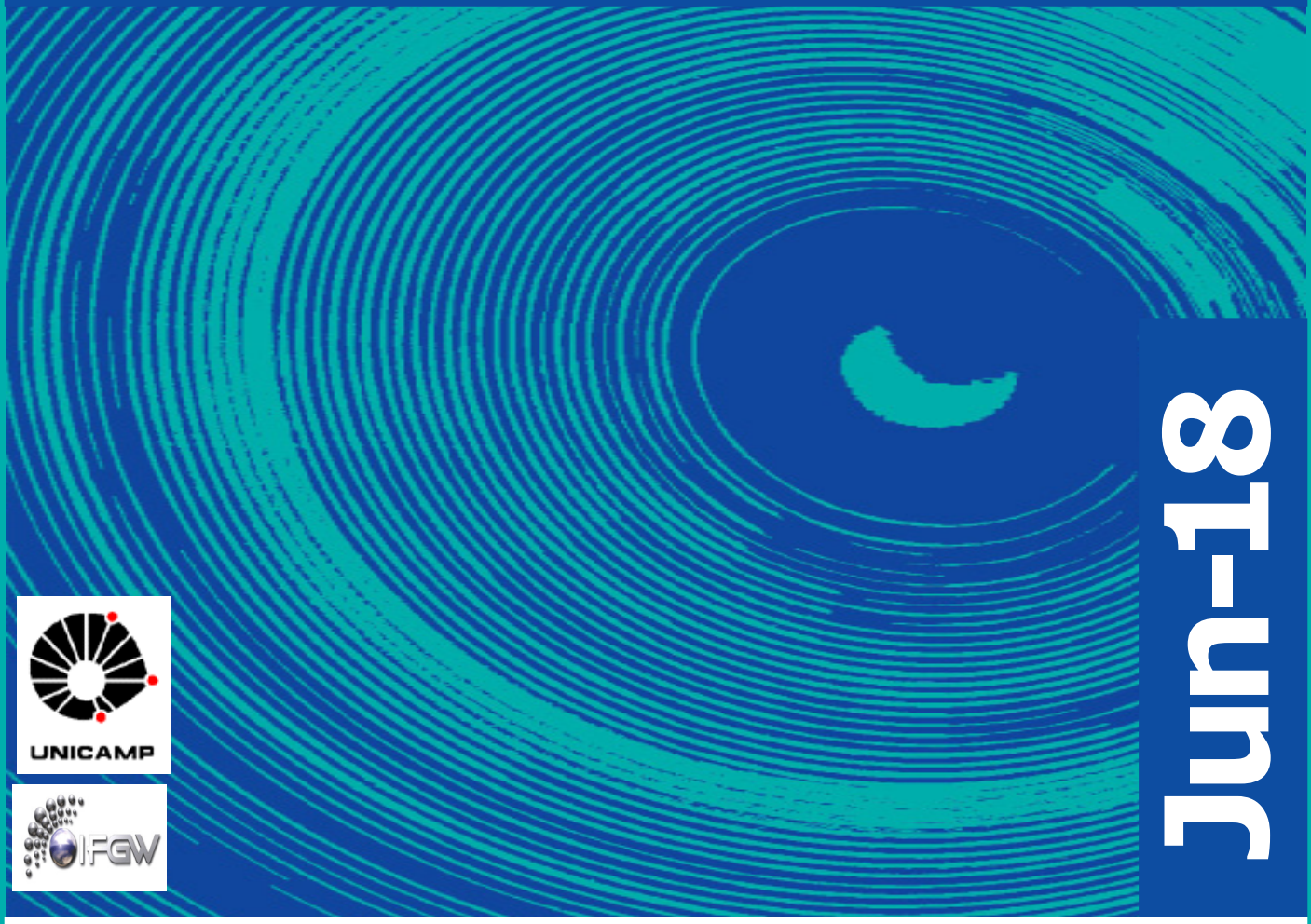

Jun-18

UNICAMP

IFGW

Artigos publicados - P092-2018 à P189-2018

Meeting Abstract - Me001-2018

Correções - Co003-2018

Defesas de Dissertações do IFGW - D008-2018 à D009-2018

Defesas de Teses do IFGW - T011-2018 à T012-2018

Artigos publicados

[P092-2018] "3D Printed e-Tongue"

Gaal, G.*; da Silva, T. A.*; Gaal, V.*; Hensel, R. C.*; Amaral, L. R.; **Rodrigues, V.*; Riul, A.***

Nowadays, one of the biggest issues addressed to electronic sensor fabrication is the build-up of efficient electrodes as an alternative way to the expensive, complex and multistage processes required by traditional techniques. Printed electronics arises as an interesting alternative to fulfill this task due to the simplicity and speed to stamp electrodes on various surfaces. Within this context, the Fused Deposition Modeling 3D printing is an emerging, cost-effective and alternative technology to fabricate complex structures that potentiates several fields with more creative ideas and new materials for a rapid prototyping of devices. We show here the fabrication of interdigitated electrodes using a standard home-made CoreXY 3D printer using transparent and graphene-based PLA filaments. Macro 3D printed electrodes were easily assembled within 6 min with outstanding reproducibility. The electrodes were also functionalized with different nanostructured thin films via dip-coating Layer-by-Layer technique to develop a 3D printed e-tongue setup. As a proof of concept, the printed e-tongue was applied to soil analysis. A control soil sample was enriched with several macro-nutrients to the plants (N, P, K, S, Mg, and Ca) and the discrimination was done by electrical impedance spectroscopy of water solution of the soil samples. The data was analyzed by Principal Component Analysis and the 3D printed sensor distinguished clearly all enriched samples despite the complexity of the soil chemical composition. The 3D printed e-tongue successfully used in soil analysis encourages further investments in developing new sensory tools for precision agriculture and other fields exploiting the simplicity and flexibility offered by the 3D printing techniques.

FRONTIERS IN CHEMISTRY 6, 151, 2018. DOI: 10.3389/fchem.2018.00151

[P093-2018] "A measurement of CMB cluster lensing with SPT and DES year 1 data"

Baxter, E. J.; Raghunathan, S.; Crawford, T. M.; **Sobreira, F.***; et al.

Clusters of galaxies gravitationally lens the cosmic microwave background (CMB) radiation, resulting in a distinct imprint in the CMB on arcminute scales. Measurement of this effect offers a promising way to constrain the masses of galaxy clusters, particularly those at high redshift. We use CMB maps from the South Pole Telescope Sunyaev-Zel'dovich (SZ) survey to measure the CMB lensing signal around galaxy clusters identified in optical imaging from first year observations of the Dark Energy Survey. The cluster catalogue used in this analysis contains 3697 members with mean redshift of (z) over bar = 0.45. We detect lensing of the CMB by the galaxy clusters at 8.1 sigma significance. Using the measured lensing signal, we constrain the amplitude of the relation between cluster mass and optical richness to roughly 17 per cent precision, finding good agreement with recent constraints obtained with galaxy lensing. The error budget is dominated by statistical noise but includes significant contributions from systematic biases due to the thermal SZ effect and cluster miscentring.

MONTHLY NOTICES OF THE ROYAL ASTRONOMICAL SOCIETY 476 [2], 2674-2688, 2018. DOI: 10.1093/mnras/sty305

[P094-2018] "A novel copper precursor for electron beam induced deposition"

Haverkamp, C.; Sarau, G.; Polyakov, M. N.; Utke, I.; **dos Santos, M. V. P.***; Christiansen, S.; Hoflich, K.

A fluorine free copper precursor, Cu(tbaoac)(2) with the chemical sum formula CuC16O6H26 is introduced for focused electron beam induced deposition (FEBID). FEBID with 15 keV and 7 nA results in deposits with an atomic composition of Cu: O:C of approximately 1: 1:2. Transmission electron microscopy proved that pure copper nanocrystals with sizes of up to around 15 nm were dispersed inside the carbonaceous matrix. Raman investigations revealed a high degree of amorphization of the carbonaceous matrix and showed hints for partial copper oxidation taking place selectively on the surfaces of the deposits. Optical transmission/reflection measurements of deposited pads showed a dielectric behavior of the material in the optical spectral range. The general behavior of the permittivity could be described by applying the Maxwell-Garnett mixing model to amorphous carbon and copper. The dielectric function measured from deposited pads was used to simulate the optical response of tip arrays fabricated out of the same precursor and showed good agreement with measurements. This paves the way for future plasmonic applications with copper-FEBID.

BEILSTEIN JOURNAL OF NANOTECHNOLOGY 9, 1220-1227, 2018. DOI: 10.3762/bjnano.9.113

[P095-2018] "A T-shaped double quantum dot system as a Fano interferometer: Interplay of coherence and correlation upon spin currents"

Fernandes, I. L.*; Cabrera, G. G.*

Based on Keldysh non-equilibrium Green function method, we have investigated spin current production in a hybrid T-shaped device, consisting of a central quantum dot connected to the leads and a side dot which only couples to the central dot. The topology of this structure allows for quantum interference of the different paths that go across the device, yielding Fano resonances in the spin dependent transport properties. Correlation effects are taken into account at the central dot and handled within a mean field approximation. Its interplay with the Fano effect is analyzed in the strong coupling regime. Non-vanishing spin currents are only obtained when the leads are ferromagnetic, the current being strongly dependent on the relative orientation of the lead polarizations. We calculate the conductance (spin and charge) by numerically differentiating the current, and a rich structure is obtained as a manifestation of quantum coherence and correlation effects. Increase of the Coulomb interaction produces localization of states at the side dot, largely suppressing Fano resonances. The interaction is also responsible for the negative values of the spin conductance in some regions of the voltage near resonances, effect which is the spin analog of the Esaki tunnel diode. We also analyze control of the currents via gate voltages applied to the dots, possibility which is interesting for practical operations.

PHYSICA E-LOW-DIMENSIONAL SYSTEMS & NANOSTRUCTURES 99, 98-105, 2018. DOI: 10.1016/j.physe.2018.01.021

[P096-2018] "Antibacterial properties of chitosan-based coatings are affected by spacer-length and molecular weight"

Vaz, J. M.; Taketa, T. B.; **Hernandez-Montelongo, J.***; Chevallier, P.; **Cotta, M. A.***; Mantovani, D.; Beppu, M. M.

Chitosan is a biopolymer with antibacterial properties, which are dependent on its molecular weight (Mw) and its degree of deacetylation (DDA). When grafted on surfaces as a coating, chitosan antibacterial efficiency is also dependent on the polymer chain conformation on the surface, as the amine groups, responsible of the antibacterial effect, should be available for contact with bacteria.

To investigate this behavior, chitosans with different Mw were grafted onto plasma aminated surfaces through three different spacers: glutaric anhydride (GA), poly(ethylene-glycol) bis(carboxymethyl) ether (PEGb), and poly (ethylene-alt--maleic anhydride) (PA). The grafting efficiency was evaluated by X-ray Photoelectron Spectroscopy (XPS), contact angle and Rose Bengal test, while morphological features were assessed by profilometry analyses. Results evidenced a clear influence of the anchor arm length and of the Mw of chitosan both on the grafting efficiency and on the antibacterial behavior. PA CHIMW surface exhibited a better antibacterial response compared to GA and PEGb, which could be correlated to a denser coating coverage as seen by XPS and profilometry results. Further, PA CHIMW coating displayed a higher amine density, thus promoting the interaction with the bacteria cell wall. Based on these results, chitosan-based coatings can then be extended to a wide range of antibacterial applications.

APPLIED SURFACE SCIENCE 445, 478-487, 2018. DOI: 10.1016/j.apsusc.2018.03.110

[P097-2018] "Association between hemodynamic activity and motor performance in six-month-old full-term and preterm infants: a functional near-infrared spectroscopy study"

de Oliveira, S. R.; Machado, A. C. C. D.; de Paula, J. J.; de Moraes, P. H. P.; Nahin, M. J. S.; Magalhaes, L. D.; **Novi, S. L.*; Mesquita, R. C.***; de Miranda, D. M.; Bouzada, M. C. F.

This study aimed to assess task-induced activation in motor cortex and its association with motor performance in full-term and preterm born infants at six months old. A cross-sectional study of 73 sixmonth- old infants was conducted (35 full-term and 38 preterm infants). Motor performance was assessed using the Bayley Scales of Infant Development third edition--Bayley-III. Brain hemodynamic activity during motor task was measured by functional near-infrared spectroscopy (fNIRS). Motor performance was similar in full-term and preterm infants. However, differences in hemodynamic response were identified. Full terms showed a more homogeneous unilateral and contralateral activated area, whereas in preterm-born the activation response was predominantly bilateral. The full--term group also exhibited a shorter latency for the hemodynamic response than the preterm group. Hemodynamic activity in the left sensorimotor region was positively associated with motor performance measured by Bayley-III. The results highlight the adequacy of fNIRS to assess differences in task--induced activation in sensorimotor cortex between groups. The association between motor performance and the hemodynamic activity require further investigation and suggest that fNIRS can become a suitable auxiliary tool to investigate aspects of neural basis on early development of motor abilities.

NEUROPHOTONICS 5[1], 011016, 2018. DOI: 10.1117/1.NPh.5.1.011016

[P098-2018] "Axion dark matter in a 3-3-1 model"

Montero, J. C.; **Castellanos, A. R. R.*; Sanchez-Vega, B. L.***

Slightly extending a right-handed neutrino version of the 3 - 3 - 1 model, we show that it is not only possible to solve the strong CP problem but also to give the total dark matter abundance reported by the Planck collaboration. Specifically, we consider the possibility of introducing a 3 - 3 - 1 scalar singlet to implement a gravity stable Peccei-Quinn mechanism in this model. Remarkably, for allowed regions of the parameter space, the arising axions with masses m(a) approximate to meV can both make up the total dark matter relic density through nonthermal production mechanisms and be very close to the region to be explored by the IAXO helioscope.

PHYSICAL REVIEW D 97[6], 063015, 2018. DOI: 10.1103/PhysRevD.97.063015

[P099-2018] "Combination of inclusive and differential t(t) over-bar charge asymmetry measurements using ATLAS and CMS data at root S =7 and 8 TeV"

Aaboud, M.; Aad, G.; Abbott, B.; **Chinellato, J. A.*; Tonelli Manganote, E. J.***; et al.
ATLAS Collaboration; ATLAS Collaboration; CMS Collaboration

This paper presents combinations of inclusive and differential measurements of the charge asymmetry (A(C)) in top quark pair (t(t)over-bar) events with a lepton+jets signature by the ATLAS and CMS Collaborations, using data from LHC proton-proton collisions at centre-of-mass energies of 7 and 8 TeV. The data correspond to integrated luminosities of about 5 and 20 fb(-1) for each experiment, respectively. The resulting combined LHC measurements of the inclusive charge asymmetry are A(C) (LHC7) = 0.005 +/- 0.007 (stat) +/- 0.006 (syst) at 7 TeV and A(C) (LHC8) = 0.0055 +/- 0.0023 (stat) +/- 0.0025 (syst) at 8 TeV. These values, as well as the combination of A(C)measurements as a function of the invariant mass of the t(t)over-bar system at 8 TeV, are consistent with the respective standard model predictions.

JOURNAL OF HIGH ENERGY PHYSICS [4], 033, 2017. DOI: 10.1007/JEHPO4(2018)033

[P100-2018] "Combined search for electroweak production of charginos and neutralinos in proton-proton collisions at root s=13 TeV"

Sirunyan, A. M.; Tumasyan, A.; Adam, W.; **Chinellato, J. A.*; Tonelli Manganote, E. J.*;** et al.
CMS Collaboration

A statistical combination of several searches for the electroweak production of charginos and neutralinos is presented. All searches use proton-proton collision data at A root s = 13 TeV, recorded with the CMS detector at the LHC in 2016 and corresponding to an integrated luminosity of 35.9 fb(-1). In addition to the combination of previous searches, a targeted analysis requiring three or more charged leptons (electrons or muons) is presented, focusing on the challenging scenario in which the difference in mass between the two least massive neutralinos is approximately equal to the mass of the Z boson. The results are interpreted in simplified models of chargino-neutralino or neutralino pair production. For chargino-neutralino production, in the case when the lightest neutralino is massless, the combination yields an observed (expected) limit at the 95% confidence level on the chargino mass of up to 650 (570) GeV, improving upon the individual analysis limits by up to 40 GeV. If the mass difference between the two least massive neutralinos is approximately equal to the mass of the Z boson in the chargino-neutralino model, the targeted search requiring three or more leptons obtains observed and expected exclusion limits of around 225 GeV on the second neutralino mass and 125 GeV on the lightest neutralino mass, improving the observed limit by about 60 GeV in both masses compared to the previous CMS result. In the neutralino pair production model, the combined observed (expected) exclusion limit on the neutralino mass extends up to 650-750 (550-750) GeV, depending on the branching fraction assumed. This extends the observed exclusion achieved in the individual analyses by up to 200 GeV. The combined result additionally excludes some intermediate gaps in the mass coverage of the individual analyses.

JOURNAL OF HIGH ENERGY PHYSICS [3], 160, 2018. DOI: 10.1007/JHEP03(2018)160

[P101-2018] "Comparing transverse momentum balance of b jet pairs in pp and PbPb collisions at root s(NN)=5.02 TeV"

Sirunyan, A. M.; Tumasyan, A.; Adam, W.; **Chinellato, J. A.*; Tonelli Manganote, E. J.***; et al.
CMS Collaboration

The transverse momentum balance of pairs of back-to--back b quark jets in PbPb and pp collisions recorded with the CMS detector at the LHC is reported. The center-of--mass energy in both collision systems is 5.02 TeV per nucleon pair. Compared to the pp collision baseline, b quark jets have a larger imbalance in the most central PbPb collisions, as expected from the jet quenching effect. The data are also compared to the corresponding measurement with inclusive dijets. In the most central collisions, the imbalance of b quark dijets is comparable to that of inclusive dijets.

JOURNAL OF HIGH ENERGY PHYSICS 3, 181, 2018. DOI: 10.1007/JHEP03(2018)181

[P102-2018] "Constraints on the chiral magnetic effect using charge-dependent azimuthal correlations in pPb and PbPb collisions at the CERN Large Hadron Collider"

Sirunyan, A. M.; Tumasyan, A.; Adam, W.; **Chinellato, J. A.*; Tonelli Manganote, E. J.***; et al.
CMS Collaboration

Charge-dependent azimuthal correlations of same-and opposite-sign pairs with respect to the second-and third-order event planes have been measured in pPb collisions at root s(NN) = 8.16 TeV and PbPb collisions at 5.02 TeV with the CMS experiment at the LHC. The measurement is motivated by the search for the charge separation phenomenon predicted by the chiral magnetic effect (CME) in heavy ion collisions. Three-and two-particle azimuthal correlators are extracted as functions of the pseudorapidity difference, the transverse momentum (p(T)) difference, and the p(T) average of same-and opposite-charge pairs in various event multiplicity ranges. The data suggest that the charge-dependent three-particle correlators with respect to the second-and third-order event planes share a common origin, predominantly arising from charge-dependent two-particle azimuthal correlations coupled with an anisotropic flow. The CME is expected to lead to a v(2)-independent three-particle correlation when the magnetic field is fixed. Using an event shape engineering technique, upper limits on the v(2)-independent fraction of the three-particle correlator are estimated to be 13% for pPb and 7% for PbPb collisions at 95% confidence level. The results of this analysis, both the dominance of two--particle correlations as a source of the three-particle results and the similarities seen between PbPb and pPb, provide stringent constraints on the origin of charge-dependent three-particle azimuthal correlations and challenge their interpretation as arising from a chiral magnetic effect in heavy ion collisions.

PHYSICAL REVIEW C 97[4], 044912, 2018. DOI: 10.1103/PhysRevC.97.044912

[P103-2018] "Coupling of phonons with orbital dynamics and magnetism in CuSb2O6"

Maimone, D. T.*; Christian, A. B.; Neumeier, J. J.; **Granado, E.***

Strongly interacting phonons and orbital excitations are observed in the same energy range for CuSb2O6, unlocking a so-far unexplored type of electron-phonon interaction. An orbital wave at similar to 550 cm(-1) softens on warming and strongly interferes with a phonon at similar to 500 cm(-1), giving rise to a merged excitation of mixed character. An electronic continuum grows on warming to the orbital ordering temperature T-oo = 400 K, generating an important phonon decay channel. This direct and simultaneous observation of orbital and vibrational excitations reveals details of their combined dynamics. In addition, phonon frequency anomalies due to magnetic correlations are observed below similar to 150 K, much above the three-dimensional magnetic ordering temperature T-N(3D) = 8.5 K, confirming one-dimensional magnetic correlations along Cu-O-O-Cu linear chains in the paramagnetic state.

PHYSICAL REVIEW B 97[17], 174415, 2018. DOI: 10.1103/PhysRevB.97.174415

[P104-2018] "Dark Energy Survey Year 1 results: curved-sky weak lensing mass map"

Chang, C.; Pujol, A.; Mawdsley, B.; **Sobreira, F.***; et al.
DES Collaboration

We construct the largest curved-sky galaxy weak lensing mass map to date from the DES first-year (DES Y1) data. The map, about 10 times larger than the previous work, is constructed over a contiguous approximate to 1500 deg(2), covering a comoving volume of approximate to 10 Gpc(3). The effects of masking, sampling, and noise are tested using simulations. We generate weak lensing maps from two DES Y1 shear catalogues, METACALIBRATION and IM3SHAPE, with sources at red--shift 0.2 < z < 1.3, and in each of four bins in this range. In the highest signal-to-noise map, the ratio between the mean signal to noise in the E-mode map and the B-mode map is similar to 1.5 (similar to 2) when smoothed with a Gaussian filter of sigma(G) = 30 (80) arcmin. The second and third moments of the convergence kappa in the maps are in agreement with simulations. We also find no significant correlation of kappa with maps of potential systematic contaminants. Finally, we demonstrate two applications of the mass maps: (1) cross--correlation with different foreground tracers of mass and (2) exploration of the largest peaks and voids in the maps.

MONTHLY NOTICES OF THE ROYAL ASTRONOMICAL SOCIETY 475[3], 3165-3190, 2018. DOI: 10.1093/mnras/stx3363

[P105-2018] "Dark Energy Survey Year 1 results: the impact of galaxy neighbours on weak lensing cosmology with IM3SHAPE"

Samuroff, S.; Bridle, S. L.; Zuntz, J.; **Sobreira, F.***; et al.
DES Collaboration

We use a suite of simulated images based on Year 1 of the Dark Energy Survey to explore the impact of galaxy neighbours on shape measurement and shear cosmology. The HOOPOE image simulations include realistic blending, galaxy positions, and spatial variations in depth and point spread function properties. Using the IM3SHAPE maximum-likelihood shape measurement code, we identify four mechanisms by which neighbours can have a non-negligible influence on shear estimation. These effects, if ignored, would contribute a net multiplicative bias of m similar to 0.03-0.09 in the Year One of the Dark Energy Survey (DES Y1) IM3SHAPE catalogue, though the precise impact will be dependent on both the measurement code and the selection cuts applied. This can be reduced to percentage level or less by removing objects with close neighbours, at a cost to the effective number density of galaxies n(eff) of 30 per cent. We use the cosmological inference pipeline of DES Y1 to explore the cosmological implications of neighbour bias and show that omitting blending from the calibration simulation for DES Y1 would bias the inferred clustering amplitude S-8 equivalent to sigma(8)(Omega(m)/0.3)(0.5) by 2 sigma towards low values. Finally, we use the HOOPOE simulations to test the effect of neighbour-induced spatial correlations in the multiplicative bias.

We find the impact on the recovered S-8 of ignoring such correlations to be subdominant to statistical error at the current level of precision.

MONTHLY NOTICES OF THE ROYAL ASTRONOMICAL SOCIETY 475[4], 4524-4543, 2018. DOI: 10.1093/mnras/stx3282

[P106-2018] "Dark Energy Survey Year 1 Results: The Photometric Data Set for Cosmology"

Drlica-Wagner, A.; Sevilla-Noarbe, I.; Rykoff', E. S.; **Sobreira, F.***; et al.
DES Collaboration

We describe the creation, content, and validation of the Dark Energy Survey (DES) internal year-one cosmology data set, Y1A1 GOLD, in support of upcoming cosmological analyses. The Y1A1 GOLD data set is assembled from multiple epochs of DES imaging and consists of calibrated photometric zero-points, object catalogs, and ancillary data products-e.g., maps of survey depth and observing conditions, star galaxy classification, and photometric redshift estimates that are necessary for accurate cosmological analyses. The Y1A1 GOLD wide area object catalog consists of similar to 137 million objects detected in co-added images covering similar to 1800 deg(2) in the DES grizY filters. The 10 sigma limiting magnitude for galaxies is g = 23.4, r = 23.2, i = 22.5, z = 21.8, and Y = 20.1. Photometric calibration of Y1A1 GOLD was performed by combining nightly zero-point solutions with stellar locus regression, and the absolute calibration accuracy is better than 2% over the survey area. DES Y1A1 GOLD is the largest photometric data set at the achieved depth to date, enabling precise measurements of cosmic acceleration at z less than or similar to 1.

ASTROPHYSICAL JOURNAL SUPPLEMENT SERIES 235[2], 33, 2018. DOI: 10.3847/1538-4365/aab4f5

[P107-2018] "Deformation Mechanisms of Vertically Stacked WS2/MoS2 Heterostructures: The Role of Interfaces"

Susarla, S.; Manimunda, P.; **Jaques, Y. M.***; Hachtel, J. A.; Idrobo, J. C.; Amnulla, S. A. S.; **Galvao, D. S.***; Tiwary, C. S.; Ajayan, P. M.

The mechanical and optical properties generated due to the stacking of different atomically thin materials have made it possible to tune and engineer these materials for next-generation electronics. The understanding of the interlayer interactions in such stacked structures is of fundamental interest for structure and property correlation. Here, a combined approach of in situ Raman spectroscopy and mechanical straining along with molecular dynamics (MD) simulations has been used to probe one such interface, namely, the WS2/MoS2 heterostructure. Vertical heterostructures on poly(methyl methacrylate), when flexed, showed signs of decoupling at 1.2% strain. Theoretical calculations showed strain induced stacking changes at 1.75% strain. The sliding characteristics of layers were also investigated using scanning probe microscopy based nanoscratch testing, and the results are further supported by MD simulations. The present study could be used to design future optoelectronic devices based on WS2/MoS2 heterostructures.

ACS NANO 12[4], 4036-4044, 2018. DOI: 10.1021/acsnano.8b01786

[P108-2018] "Delaying fat bloom formation in dark chocolate by adding sorbitan monostearate or cocoa butter stearin"

Buscato, M. H. M.; Hara, L. M.; Bonomi, E. C.; **Calligaris, G. D.*; Cardoso, L. P.***; Grimaldi, R.; Kieckbusch, T. G.

Two formulations of dark chocolate were developed by adding cocoa butter stearin (CBSt) or sorbitan monostearate (SMS) and compared to a standard formulation in order to investigate fat bloom formation over time. Fat bloom was monitored by Whiteness Index (WI), melting behavior and polymorphism determinations, in bars stored during 90 days at 20 degrees C and under oscillating temperature between 20 and 32 degrees C. All samples stored at 20 degrees C did not develop fat bloom and the required beta(V) form was maintained. Under oscillating storage condition, samples with CBSt (6.0%, w/w) and SMS (0.15%, w/w) delayed the surface fat bloom formation by at least 45 and 15 days, respectively, compared to standard chocolate, observed visually and through WI increments. The beta(V) to beta(VI) polymorphic transition correlated well with the WI, and also with changes in DSC thermograms, confirming the higher effectiveness of specific triacylglycerol (mainly StOSt) in delaying bloom formation.

FOOD CHEMISTRY 256, 390-396, 2018. DOI: 10.1016/j.foodchem.2018.02.127

[P109-2018] "Differences in hydrogen absorption over Pd and Pt functionalized CVD-grown GaN nanowires"

Prasad, A. K.; **Sahoo, P. K.***; Dhara, S.; Dash, S.; Tyagi, A. K.

In this study, we report the differences in hydrogen (H-2) absorption properties of platinum (Pt) and palladium (Pd) functionalized gallium nitride (GaN) nanowires via gas sensing studies. GaN nanowires of similar to 25 - 200 nm diameter and similar to 50 - 75 gm length are grown uniformly over large area (10 x 10 mm(2)) using Au assisted chemical vapour deposition technique. The nanowires are grown at 900 for 2 h using gallium (Ga) as source material and ammonia (NH3) as the reacting gas. The nanowires are functionalized with Pd and Pt nanoclusters using solution technique. H-2 absorption by these functionalized nanowires which is manifested as gas sensing response is compared in the temperature range of 50-200. The role of surface kinetics in Pd and Pt is shown to be responsible for the difference in the sensor response.

MATERIALS CHEMISTRY AND PHYSICS 211, 355-360, 2018. DOI: 10.1016/j.matchemphys.2018.02.034

[P110-2018] "Differences in the Mechanical Properties of Monolayer and Multilayer WSe2/MoSe2"

Jaques, Y. M.*; Manimunda, P.; Nakanishi, Y.; Susarla, S.; **Woellner, C. F.***; Bhowmick, S.; Asif, S. A. S.; **Galvao, D. S.***; Tiwary, C. S.; Ajayan, P. M.

Transition metal dichalcogenides are 2D structures with remarkable electronic, chemical, optical and mechanical properties. Monolayer and crystal properties of these structures have been extensively investigated, but a detailed understanding of the properties of their few-layer structures are still missing. In this work we investigated the mechanical differences between monolayer and multilayer WSe2 and MoSe2, through fully atomistic molecular dynamics simulations (MD). It was observed that single layer WSe2/MoSe2 deposited on silicon substrates have larger friction coefficients than 2, 3 and 4 layered structures. For all considered cases it is always easier to peel off and/or to fracture MoSe2 structures. These results suggest that the interactions between first layer and substrate are stronger than interlayer interactions themselves. Similar findings have been reported for other nanomaterials and it has been speculated whether this is a universal-like behavior for 2D layered materials. We have also analyzed fracture patterns. Our results show that fracture is chirality dependent with crack propagation preferentially perpendicular to W(Mo)-Se bonds and faster for zig-zag-like defects.

MRS ADVANCES 3[6-7], 373-378, 2018. DOI: 10.1557/adv.2018.246

[P111-2018] "Efficient prediction of suitable functional monomers for molecular imprinting via local density of states calculations"

Zink, S.; **Moura, F. A.***; Autreto, P. A. D.; **Galvao, D. S.***; Mizaikoff, B.

Synthetic molecular recognition materials, such as molecularly imprinted polymers (MIPs), are of increasing importance in biotechnology and analytical chemistry, as they are able to selectively bind their respective template. However, due to their specificity, each MIP has to be individually designed for the desired target leading to a molecularly tailored synthesis strategy. While trial-and-error remains the common approach for selecting suitable functional monomers (FMs), the study herein introduces a radically new approach towards rationally designing MIPs by rapidly screening suitable functional monomers based on local density of states (LDOS) calculations in a technique known as Electronic Indices Methodology (EIM). An EIM-based method of classification of FMs according to their suitability for imprinting was developed. Starting from a training set of nine different functional monomers, the prediction of suitability of four functional monomers was possible. These predictions were subsequently experimentally confirmed.

PHYSICAL CHEMISTRY CHEMICAL PHYSICS 20[19], 13153-13158, 2018. DOI: 10.1039/c7cp08283e

[P112-2018] "Electron-impact electronic-state excitation of para-benzoquinone"

Jones, D. B.; **da Costa, R. F.*; Kossoski, F.***; Varella, M. T. do N.; Bettega, M. H. F.; Ferreira da Silva, F.; Limao-Vieira, P.; Garcia, G.; **Lima, M. A. P.***; White, R. D.; Brunger, M. J.

Angle resolved electron energy loss spectra (EELS) for para-benzoquinone ($C_6H_4O_2$) have been recorded for incident electron energies of 20, 30, and 40 eV. Measured differential cross sections (DCSs) for electronic band features, composed of a combination of energetically unresolved electronic states, are subsequently derived from those EELS. Where possible, the obtained DCSs are compared with those calculated using the Schwinger multichannel method with pseudopotentials. These calculations were performed using a minimum orbital basis single configuration interaction framework at the static exchange plus polarisation level. Here, quite reasonable agreement between the experimental cross sections and the theoretical cross sections for the summation of unresolved states was observed. Published by AIP Publishing.

JOURNAL OF CHEMICAL PHYSICS 148[12], 124312, 2018. DOI: 10.1063/1.5023494

[P113-2018] "Electrostatic immobilization of antimicrobial peptides on polyethylenimine and their antibacterial effect against Staphylococcus epidermidis"

Hernandez-Montelongo, J.*; Corrales Urena, Y. R.; Machado, D.; Lancelloti, M.; Pinheiro, M. P.; Rischka, K.; Lisboa-Filho, P. N.; **Cotta, M. A.***

Staphylococcus epidermidis is a gram-positive bacterium, and one of the most prevalent causes of nosocomial infections due to its strong ability to form biofilms on catheters and surgical implants. Here we explore the antimicrobial properties of Tet-124 peptides, which are part of the innate defense against different multicellular organisms in nature. Two different Tet-124 peptides were immobilized on a polyethylenimine (PEI) film to determine their impact on the antimicrobial properties: KLWWMIRRW (Tet-124), which contains only natural amino acids, and KLWWMIRRWG-(F-Br)-G (F-Br- 4-Bromophenylalanine), a modified Tet-124 sequence with the addition of an unnatural amino acid. The immobilization was obtained as a result of the electrostatic interaction between PEI amino groups and the C-terminal carboxylic groups of tryptophan and glycine amino acids of Tet-124 and Tet-124-Br peptides, respectively. The process was monitored and studied by water contact angle, Atomic Force Microscopy (AFM), X-ray Photoelectron Spectroscopy (XPS) and Quartz Crystal Microbalance with Dissipation (QCM-D) measurements. The antibacterial effect of our samples against S. epidermis was evaluated by the spread plate counting method, and cytotoxicity was tested using fibroblast cultures. Our results indicate the feasibility to immobilize electrostatically both Tet-124 peptides for biomedical applications.

COLLOIDS AND SURFACES B-BIOINTERFACES 164, 370-378, 2018. DOI: 10.1016/j.colsurfb.2018.02.002

[P114-2018] "Enhanced thermal conductivity and mechanical properties of hybrid MoS2/h-BN polyurethane nanocomposites"

Ribeiro, H.; Trigueiro, J. P. C.; Lopes, M. C.; Pedrotti, J. J.; **Woellner, C. F.***; Silva, W. M.; Silva, G. G.; Ajayan, P. M.

Nanocomposites based on molybdenum disulfide (MoS_2), hexagonal boron nitride (h-BN) and hybrid MoS_2/h-BN nanofillers with different wt % in elastomeric polyurethane (PU) were studied with respect to their microstructure, thermal and mechanical properties. Tensile tests showed increases up to 80% in Young`s modulus for both h-BN and hybrid MoS_2/h-BN composites. These results agree with dynamic mechanical analysis tests, which confirm an increase of up to 106% in storage modulus for hybrid MoS_2/h-BN with 0.5 wt % content. When the hybrid MoS_2/h-BN nanofillers were incorporated into the polymeric matrix, increases up to 102% in crosslink density were observed, indicating that strong interactions between the hybrid nanofillers and PU were established. However, the most important synergistic effect between the mixture of MoS_2 and h-BN nanoadditives was the increase of up to 752% in thermal conductivity with respect to neat polymer. Therefore, hybrid composites based in two-dimensional MoS_2/h-BN nanofillers with multifunctional attributes can be applied in advanced polymeric materials that require high mechanical and thermal performance.

JOURNAL OF APPLIED POLYMER SCIENCE 135[30], 46560, 2018. DOI: 10.1002/app.46560

[P115-2018] "Experimental and computational investigation of reduced graphene oxide nanoplatelets stabilized in poly(styrene sulfonate) sodium salt"

Miyazaki, C. M.; **Maria, M. A. E.*; Borges, D. D.*; Woellner, C. F.*; Brunetto, G.*; Fonseca, A. F.***; Constantino, C. J. L.; Pereira-da-Silva, M. A.; **de Siervo, A.*; Galvao, D. S.*; Riul, A.***

The production of large-area interfaces and the use of scalable methods to build up designed nanostructures generating advanced functional properties are of high interest for many materials science applications. Nevertheless, large-area coverage remains a major problem even for pristine graphene, and here we present a hybrid, composite graphene-like material soluble in water that can be exploited in many areas such as energy storage, electrodes fabrication, selective membranes and biosensin. Graphene oxide (GO) was produced by the traditional Hummers' method being further reduced in the presence of poly(styrene sulfonate) sodium salt (PSS), thus creating stable reduced graphene oxide (rGO) nanoplatelets wrapped by PSS (GPSS).

Molecular dynamics simulations were carried out to further clarify the interactions between PSS molecules and rGO nanoplatelets, with calculations supported by Fourier transform infrared spectroscopy analysis. The intermolecular forces between rGO nanoplatelets and PSS lead to the formation of a hybrid material (GPSS) stabilized by van der Waals forces, allowing the fabrication of high-quality layer-by-layer (LbL) films with poly(allylamine hydrochloride) (PAH). Raman and electrical characterizations corroborated the successful modifications in the electronic structures from GO to GPSS after the chemical treatment, resulting in (PAH/GPSS) LbL films four orders of magnitude more conductive than (PAH/GO).

JOURNAL OF MATERIALS SCIENCE 53[14], 10049-10058, 2018. DOI: 10.1007/s10853-018-2325-1

[P116-2018] "Formation of Ag nanoparticles under electron beam irradiation: Atomistic origins from first-principles calculations"

Andres, J.; Gouveia, A. F.; Gracia, L.; Longo, E.; Faccin, G.; **Silva, E. Z.***; Pereira, D. H.; San-Miguel, M. A.

The formation of Ag nanoparticles is currently a topic subject to a great deal of research because they are excellent materials with many technological applications. Recently, the formation of Ag nanoparticles on -Ag2WO4 semiconductors induced by electron irradiation has been reported, but the mechanism underlying the transformations remains elusive. The aim of this article is to describe the mechanisms of electron beam irradiation on -Ag2WO4 and its transformation to form Ag nanoparticles in vacuum conditions. To this end, a combined study involving experiments and multiscale computational approaches (density functional theory calculations and molecular dynamics simulations) is presented. With the increasing interplay between experimental and computational approaches at multiple length scales, we will also discuss how these combined data can be used to provide a deep insight into the rationalization of electron beam-induced transformations. This phenomenon is likely to be promoted by electron charge redistribution in these materials due to electronic excitations combined with the formation of silver vacancies under electron beam irradiation. As this mechanism should be relevant to other Ag-based materials, our results provide pointers for the further development and optimization of electron beam-mediated engineering of the atomic structure and electronic properties at the atomic resolution.

INTERNATIONAL JOURNAL OF QUANTUM CHEMISTRY 118[9], SI, e25551, 2018. DOI: 10.1002/qua.25551

[P117-2018] "From Weakly Chaotic Dynamics to Deterministic Subdiffusion via Copula Modeling"

Naze, P.*

Copula modeling consists in finding a probabilistic distribution, called copula, whereby its coupling with the marginal distributions of a set of random variables produces their joint distribution. The present work aims to use this technique to connect the statistical distributions of weakly chaotic dynamics and deterministic subdiffusion. More precisely, we decompose the jumps distribution of Geisel-Thomae map into a bivariate one and determine the marginal and copula distributions respectively by infinite ergodic theory and statistical inference techniques. We verify therefore that the characteristic tail distribution of subdiffusion is an extreme value copula coupling Mittag-Leffler distributions. We also present a method to calculate the exact copula and joint distributions in the case where weakly chaotic dynamics and deterministic subdiffusion statistical distributions are already known. Numerical simulations and consistency with the dynamical aspects of the map support our results.

JOURNAL OF STATISTICAL PHYSICS 171[3], 434-448, 2018. DOI: 10.1007/s10955-018-1999-8

[P118-2018] "Hybrid nanomembrane-based capacitors for the determination of the dielectric constant of semiconducting molecular ensembles"

Petrini, P. A.; Silva, R. M. L.; de Oliveira, R. F.; **Merces, L.*; Bufon, C. C. B.***

Considerable advances in the field of molecular electronics have been achieved over the recent years. One persistent challenge, however, is the exploitation of the electronic properties of molecules fully integrated into devices. Typically, the molecular electronic properties are investigated using sophisticated techniques incompatible with a practical device technology, such as the scanning tunneling microscopy. The incorporation of molecular materials in devices is not a trivial task as the typical dimensions of electrical contacts are much larger than the molecular ones. To tackle this issue, we report on hybrid capacitors using mechanically-compliant nanomembranes to encapsulate ultrathin molecular ensembles for the investigation of molecular dielectric properties. As the prototype material, copper (II) phthalocyanine (CuPc) has been chosen as information on its dielectric constant (k(CuPc)) at the molecular scale is missing. Here, hybrid nanomembrane-based capacitors containing metallic nanomembranes, insulating Al2O3 layers, and the CuPc molecular ensembles have been fabricated and evaluated. The Al2O3 is used to prevent short circuits through the capacitor plates as the molecular layer is considerably thin (< 30 nm). From the electrical measurements of devices with molecular layers of different thicknesses, the CuPc dielectric constant has been reliably determined (k(CuPc) = 4.5 +/- 0.5). These values suggest a mild contribution of the molecular orientation on the CuPc dielectric properties. The reported nanomembrane-based capacitor is a viable strategy for the dielectric characterization of ultrathin molecular ensembles integrated into a practical, real device technology.

NANOTECHNOLOGY 29[26], 265201, 2018. DOI: 10.1088/1361-6528/aabc44

[P119-2018] "Identification of heavy-flavour jets with the CMS detector in pp collisions at 13 TeV"

Sirunyan, A. M.; Tumasyan, A.; Adam, W.; **Chinellato, J. A.*; Tonelli Manganote, E. J.***; et al.
CMS Collaboration

Many measurements and searches for physics beyond the standard model at the LHC rely on the efficient identification of heavy-flavour jets, i.e. jets originating from bottom or charm quarks. In this paper, the discriminating variables and the algorithms used for heavy-flavour jet identification during the first years of operation of the CMS experiment in proton-proton collisions at a centre-of-mass energy of 13 TeV, are presented. Heavy-flavour jet identification algorithms have been improved compared to those used previously at centre-of-mass energies of 7 and 8 TeV. For jets with transverse momenta in the range expected in simulated t (t) over bar events, these new developments result in an efficiency of 68% for the correct identification of a b jet for a probability of 1% of misidentifying a light-flavour jet. The improvement in relative efficiency at this misidentification probability is about 15%, compared to previous CMS algorithms. In addition, for the first time algorithms have been developed to identify jets containing two b hadrons in Lorentz-boosted event topologies, as well as to tag c jets. The large data sample recorded in 2016 at a centre--of-mass energy of 13 TeV has also allowed the development of new methods to measure the efficiency and misidentification probability of heavy-flavour jet identification algorithms.

The b jet identification efficiency is measured with a precision of a few per cent at moderate jet transverse momenta (between 30 and 300 GeV) and about 5% at the highest jet transverse momenta (between 500 and 1000 GeV).

JOURNAL OF INSTRUMENTATION 13, P05011, 2018. DOI: 10.1088/1748-0221/13/05/P05011

[P120-2018] "Improving Graphene-metal Contacts: Thermal Induced Polishing"

Oliveira, E. F.*; dos Santos, R. P. B.; **Antreto, P. A. D.***; Moshkalev, S.; **Galvao, D. S.***

Graphene is a very promising material for nanoelectronics applications due to its unique and remarkable electronic and thermal properties. However, when deposited on metallic electrodes the overall thermal conductivity is significantly decreased. This phenomenon has been attributed to the mismatch between the interfaces and contact thermal resistance. Experimentally, one way to improve the graphene/metal contact is thorough high--temperature annealing, but the detailed mechanisms behind these processes remain unclear. In order to address these questions, we carried out fully atomistic reactive molecular dynamics simulations using the ReaxFF force field to investigate the interactions between multi-layer graphene and metallic electrodes (nickel) under (thermal) annealing. Our results show that the annealing induces an upward-downward movement of the graphene layers, causing a pile-driver-like effect over the metallic surface. This graphene induced movements cause a planarization (thermal polishing-like effect) of the metallic surface, which results in the increase of the effective graphene/metal contact area. This can also explain the experimentally observed improvements of the thermal and electric conductivities.

MRS ADVANCES 3[1-2], 73-78, 2018. DOI: 10.1557/adv.2018.66

[P121-2018] "Jet properties in PbPb and pp collisions at root S-NN=5.02 TeV"

Sirunyan, A. M.; Tumasyan, A.; Adam, W.; **Chinellato, J. A.*; Tonelli Manganote, E. J.***; et al.
CMS Collaboration

Modifications of the properties of jets in PbPb collisions, relative to those in pp collisions, are studied at a nucleon-nucleon center-of-mass energy of,root S-NN = 5.02 TeV via correlations of charged particles with the jet axis in relative pseudorapidity (Delta eta), relative azimuth (Delta phi), and relative angular distance from the jet axis Delta r = root(Delta eta)(2) + (Delta phi)(2). This analysis uses data collected with the CMS detector at the LHC, corresponding to integrated luminosities of 404 mu b(-1) and 27.4 pb(-1) for PbPb and pp collisions, respectively. Charged particle number densities, jet fragmentation functions, and jet shapes are presented as a function of PbPb collision centrality and charged-particle track transverse momentum, providing a differential description of jet modifications due to interactions with the quark gluon plasma.

JOURNAL OF HIGH ENERGY PHYSICS [5], 006, 2018. DOI: 10.1007/JHEP05(2018)006

[P122-2018] "Kondo temperature and Heavy Fermion behavior in Yb1-xYxCuAl series of alloys"

Rojas, D. P.; **Gandra, F. G.***; Medina, A. N.; Fernandez Barquin, L.; Gomez Sal, J. C.

Results on x-ray diffraction, electrical resistivity, specific heat and magnetization on the Yb1-xYxCuAl series of compounds are reported. The analysis of the x-ray data shows the increase of the unit cell volume with the Y dilution. The electrical resistivity shows an evolution from Kondo lattice regime for x <= 0.6 to single impurity behavior for x = 0.8 and 0.94. The electronic coefficient. shows values of Heavy Fermion systems along the series for 0 <= x< 1. On the other hand, dc magnetic susceptibility measurements show typical curves of intermediate valence systems with a maximum around 25 K. Below this maximum, the values of low temperature susceptibility (chi (0)) decrease with the increase of Y content. From the dependence of chi (0) and chi upon Y substitution, an increase of 12% of the Kondo temperature (T-K) for x = 0.8 alloy respect to the reference YbCuAl (x = 0) is estimated. This is further supported by the evolution of the temperature of the maximum in the magnetic contribution of the specific heat. The overall results can be explained by the increase of the hybridization as consequence of negative pressure effects obtained by the chemical substitution of Yb by Y, thus leading to the increase of T-K, in agreement with the Doniach's diagram.

PHYSICA B-CONDENSED MATTER 536, 176-181, 2018. DOI: 10.1016/j.physb.2017.09.096

[P123-2018] "Lattice Boltzmann method for semiclassical fluids"

Coelho, R. C. V.; **Doria, M. M.***

We determine properties of the lattice Boltzmann method for semiclassical fluids, which is based on the Boltzmann equation and on an equilibrium distribution function given either by the Bose-Einstein or the Fermi-Dirac distributions. New D-dimensional polynomials, that generalize the Hermite ones, are introduced and we find that the weight that renders the polynomials orthonormal has to be approximately equal, or equal, to the equilibrium distribution function itself for an efficient numerical implementation of the lattice Boltzmann method. In light of the new polynomials we discuss the convergence of the series expansion of the equilibrium distribution function and the obtainment of the hydrodynamic equations. A discrete quadrature is proposed and some discrete lattices in one, two and three dimensions associated to weight functions other than the Hermite weight are obtained. We derive the forcing term for the LBM, given by the Lorentz force, which dependents on the microscopic velocity, since the bosonic and fermionic particles can be charged. Motivated by the recent experimental observations of the hydrodynamic regime of electrons in graphene, we build an isothermal lattice Boltzmann method for electrons in metals in two and three dimensions. This model is validated by means of the Riemann problem and of the Poiseuille flow. As expected for electron in metals, the Ohm's law is recovered for a system analogous to a porous medium.

COMPUTERS & FLUIDS 165, 144-159, 2018. DOI: 10.1016/j.compfluid.2018.01.019

[P124-2018] "Lepton flavor violation induced by dark matter"

Arcadi, G.; **Ferreira, C. P.***; Goertz, F.; **Guzzo, M. M.***; Queiroz, F. S.; Santos, A. C. O.

Guided by gauge principles we discuss a predictive and falsifiable UV complete model where the Dirac fermion that accounts for the cold dark matter abundance in our Universe induces the lepton flavor violation (LFV) decays mu -> e gamma and mu -> eee as well as mu - e conversion. We explore the interplay between direct dark matter detection, relic density, collider probes and lepton flavor violation to conclusively show that one may have a viable dark matter candidate yielding flavor violation signatures that can be probed in the upcoming experiments.

In fact, keeping the dark matter mass at the TeV scale, a sizable LFV signal is possible, while reproducing the correct dark matter relic density and meeting limits from direct-detection experiments.

PHYSICAL REVIEW D 97[7], 075022, 2018. DOI: 10.1103/PhysRevD.97.075022

[P125-2018] "Low-aberration beamline optics for synchrotron infrared nanospectroscopy"

Freitas, R. O.; **Deneke, C.***; Maia, F. C. B.; Medeiros, H. G.; Moreno, T.; Dumas, P.; Petroff, Y.; Westfahl, H.

Synchrotron infrared nanospectroscopy is a recently developed technique that enables new possibilities in the broadband chemical analysis of materials in the nanoscale, far beyond the diffraction limit in this frequency domain. Synchrotron infrared ports have exploited mainly the high brightness advantage provided by electron storage rings across the whole infrared range. However, optical aberrations in the beam produced by the source depth of bending magnet emission at large angles prevent infrared nanospectroscopy to reach its maximum capability. In this work we present a low-aberration optical layout specially designed and constructed for a dedicated synchrotron infrared nanospectroscopy beamline. We report excellent agreement between simulated beam profiles (from standard wave propagation and raytracing optics simulations) with experimental measurements. We report an important improvement in the infrared nanospectroscopy experiment related to the improved beamline optics. Finally, we demonstrate the performance of the nanospectroscopy endstation by measuring a hyperspectral image of a polar material and we evaluate the setup sensitivity by measuring ultra-thin polymer films down to 6 nm thick.

OPTICS EXPRESS 26[9], 11238-11249, 2018. DOI: 10.1364/OE.26.011238

[P126-2018] "MARTA: a high-energy cosmic-ray detector concept for high-accuracy muon measurement"

Abreu, P.; Andringa, S.; Assis, P.; **Dobrigkeit, C.***; et al.

A new concept for the direct measurement of muons in air showers is presented. The concept is based on resistive plate chambers (RPCs), which can directly measure muons with very good space and time resolution. The muon detector is shielded by placing it under another detector able to absorb and measure the electromagnetic component of the showers such as awater-Cherenkov detector, commonly used in air shower arrays. The combination of the two detectors in a single, compact detector unit provides a unique measurement that opens rich possibilities in the study of air showers.

EUROPEAN PHYSICAL JOURNAL C 78[4], 333, 2018. DOI: 10.1140/epjc/s10052-018-5820-2

[P127-2018] "Measurement of associated Z plus charm production in proton-proton collisions at root s=8TeV"

Sirunyan, A. M.; Tumasyan, A.; Adam, W.; **Chinellato, J. A.*; Tonelli Manganote, E. J.*;** et al.
CMS Collaboration

A study of the associated production of a Z boson and a charm quark jet (Z + c), and a comparison to production with a b quark jet (Z + b), in pp collisions at a centre-of-mass energy of 8 TeV are presented. The analysis uses a data sample corresponding to an integrated luminosity of 19.7 fb(-1), collected with the CMS detector at the CERN LHC. The Z boson candidates are identified through their decays into pairs of electrons or muons. Jets originating from heavy flavour quarks are identified using semileptonic decays of c or b flavoured hadrons and hadronic decays of charm hadrons. The measurements are performed in the kinematic region with two leptons with pT(l) > 20 GeV, vertical bar eta(l)vertical bar < 2.1, 71 < m(ll) < 111 GeV, and heavy flavour jets with p(T)(jet) > 25 GeV and vertical bar eta(jet)vertical bar < 2.5. The Z + c production cross section is measured to be sigma(pp -> Z + c + X) B(Z -> l(+)l(-)) = 8.8 +/- 0.5 (stat)+/- 0.6 (syst) pb. The ratio of the Z+c and Z+b production cross sections is measured to be sigma(pp -> Z+c+X)/sigma (pp -> Z+b+X) = 2.0 +/- 0.2 (stat)+/- 0.2 (syst). The Z+c production cross section and the cross section ratio are also measured as a function of the transverse momentum of theZ boson and of the heavy flavour jet. The measurements are compared with theoretical predictions.

EUROPEAN PHYSICAL JOURNAL C 78[4], 287, 2017. DOI: 10.1140/epjc/s10052-018-5752-x

[P128-2018] "Measurement of differential cross sections in the kinematic angular variable phi* for inclusive Z boson production in pp collisions at root s=8 TeV"

Sirunyan, A. M.; Tumasyan, A.; Adam, W.; **Chinellato, J. A.*; Tonelli Manganote, E. J.***; et al.
CMS Collaboration

Measurements of differential cross sections d sigma/d phi* and double-differential cross sections d(2)sigma/ld phi*d/y/ for inclusive Z boson production are presented using the dielectron and dimuon final states. The kinematic observable phi* correlates with the dilepton transverse momentum but has better resolution, and y is the dilepton rapidity. The analysis is based on data collected with the CMS experiment at a centre-of-mass energy of 8 TeV corresponding to an integrated luminosity of 19.7 fb(-1). The normalised cross section (1/sigma) d sigma/d phi*, within the fiducial kinematic region, is measured with a precision of better than 0.5% for phi* < 1. The measurements are compared to theoretical predictions and they agree, typically, within few percent.

JOURNAL OF HIGH ENERGY PHYSICS [3], 172, 2018. DOI: 10.1007/JHEP03(2018)172

[P129-2018] "Measurement of normalized differential t(t) over-bar cross sections in the dilepton channel from pp collisions at root s=13 TeV"

Sirunyan, A. M.; Tumasyan, A.; Adam, W.; **Chinellato, J. A.*; Tonelli Manganote, E. J.*;** et al.
CMS Collaboration

Normalized differential cross sections for top quark pair production are measured in the dilepton (e(+)e(-), mu(+)mu(-), and mu(-/+),e(+/-)) decay channels in proton-proton collisions at a center-of-mass energy of 13 TeV. The measurements are performed with data corresponding to an integrated luminosity of 2.1 fb(-1) using the CMS detector at the LHC. The cross sections are measured differentially as a function of the kinematic properties of the leptons, jets from bottom quark hadronization, top quarks, and top quark pairs at the particle and parton levels. The results are compared to several Monte Carlo generators that implement calculations up to next-to-leading order in perturbative quantum chromodynamics interfaced with parton showering, and also to fixed-order theoretical calculations of top quark pair production up to next-to-next-to-leading order.

JOURNAL OF HIGH ENERGY PHYSICS [4], 060, 2018. DOI: 10.1007/JHEP04(2018)060

[P130-2018] "Measurement of the associated production of a single top quark and a Z boson in pp collisions at, root s=13 TeV"

Sirunyan, A. M.; Tumasyan, A.; Adam, W.; **Chinellato, J. A.*; Tonelli Manganote, E. J.***; et al.
CMS Collaboration

A measurement is presented of the associated production of a single top quark and a Z boson. The study uses data from proton-proton collisions at, root s = 13 TeV recorded by the CMS experiment, corresponding to an integrated luminosity of 35.9 fb(-1). Using final states with three leptons (electrons or muons), the tZq production cross section is measured to be sigma (pp -> tZq -> Wbl(+)l(-)q) = 123(-31)(+33)(stat)(-23)(+29)(syst) fb, where l stands for electrons, muons, or tau leptons, with observed and expected significances of 3.7 and 3.1 standard deviations, respectively.

PHYSICS LETTERS B 779, 358-384, 2018. DOI: 10.1016/j.physletb.2018.02.025

[P131-2018] "Measurement of the inclusive t(t)over-bar cross section in pp collisions root s=5.02 TeV using final states with at least one charged lepton"

Sirunyan, A. M.; Tumasyan, A.; Adam, W.; **Chinellato, J. A.*; Tonelli Manganote, E. J.*;** et al.
CMS Collaboration

The top quark pair production cross section (ad) is measured for the first time in pp collisions at a center-of-mass energy of 5.02 TeV. The data were collected by the CMS experiment at the LHC and correspond to an integrated luminosity of 27.4 pb(-1). The measurement is performed by analyzing events with at least one charged lepton. The measured cross section is sigma(tt) = 69.5 +/- 6.1 (stat) +/- 5.6 (syst) +/- 1.6 (lumi) pb, with a total relative uncertainty of 12%. The result is in agreement with the expectation from the standard model. The impact of the presented measurement on the determination of the gluon distribution function is investigated.

JOURNAL OF HIGH ENERGY PHYSICS [3], 115, 2018. DOI: 10.1007/JHEP03(2018)115

[P132-2018] "Measurement of the Lambda(b) polarization and angular parameters in Lambda(b) -> J/psi Lambda decays from pp collisions at root s=7 and 8 TeV"

Sirunyan, A. M.; Tumasyan, A.; Adam, W.; **Chinellato, J. A.*; Tonelli Manganote, E. J.***; et al.
CMS Collaboration

An analysis of the bottom baryon decay Lambda(b) -> J/psi(-> mu(+)mu(-))Lambda(-> p pi(-)) is performed to measure the Lambda(b) polarization and three angular parameters in data from pp collisions at root s = 7 and 8 TeV, collected by the CMS experiment at the Large Hadron Collider. The Lambda(b) polarization is measured to be 0.00 +/- 0.06(stat) +/- 0.06(syst) and the parity-violating asymmetry parameter is determined to be 0.14 +/- 0.14(stat) +/- 0.10(syst). The measurements are compared to various theoretical predictions, including those from perturbative quantum chromodynamics.

PHYSICAL REVIEW D 97[7], 072010, 2018. DOI: 10.1103/PhysRevD.97.072010

[P133-2018] "Measurement of the Splitting Function in &ITpp &ITand Pb-Pb Collisions at root&ITsNN&IT=5.02 TeV"

Sirunyan, A. M.; Tumasyan, A.; Adam, W.; **Chinellato, J. A.*; Tonelli Manganote, E. J.*;** et al.
CMS Collaboration

Data from heavy ion collisions suggest that the evolution of a parton shower is modified by interactions with the color charges in the dense partonic medium created in these collisions, but it is not known where in the shower evolution the modifications occur. The momentum ratio of the two leading partons, resolved as subjets, provides information about the parton shower evolution. This substructure observable, known as the splitting function, reflects the process of a parton splitting into two other partons and has been measured for jets with transverse momentum between 140 and 500 GeV, in pp and PbPb collisions at a center-of-mass energy of 5.02 TeV per nucleon pair. In central PbPb collisions, the splitting function indicates a more unbalanced momentum ratio, compared to peripheral PbPb and pp collisions.. The measurements are compared to various predictions from event generators and analytical calculations.

PHYSICAL REVIEW LETTERS 120[14], 142302, 2018. DOI: 10.1103/PhysRevLett.120.142302

[P134-2018] "Mechanical Properties of Pentagraphene-based Nanotubes: A Molecular Dynamics Study"

de Sousa, J. M.*; Aguiar, A. L.; Girao, E. C.; **Fonseca, A. F.*;** Souza, A. G.; **Galvao, D. S.***

The study of the mechanical properties of nanostructured systems has gained importance in theoretical and experimental research in recent years. Carbon nanotubes (CNTs) are one of the strongest nanomaterials found in nature, with Young's Modulus (YM) in the order 1.25 TPa. One interesting question is about the possibility of generating new nanostructures with 1D symmetry and with similar and/or superior CNT properties. In this work, we present a study on the dynamical, structural, mechanical properties, fracture patterns and YM values for one class of these structures, the so-called pentagraphene nanotubes (PGNTs). These tubes are formed rolling up pentagraphene membranes (which are quasi-bidimensional structures formed by densely compacted pentagons of carbon atoms in sp(3) and sp(2) hybridized states) in the same form that CNTs are formed from rolling up graphene membranes. We carried out fully atomistic molecular dynamics simulations using the ReaxFF force field. We have considered zigzag-like and armchair-like PGNTs of different diameters. Our results show that PGNTs present E-Y similar to 800 GPa with distinct elastic behavior in relation to CNTs, mainly associated with mechanical failure, chirality dependent fracture patterns and extensive structural reconstructions.

MRS ADVANCES 3[1-2], 97-102, 2018. DOI: 10.1557/adv.2018.160

[P135-2018] "Mechanical Properties of Phagraphene Membranes: A Fully Atomistic Molecular Dynamics Investigation"

de Sousa, J. M.; Aguiar, A. L.; Girao, E. C.; **Fonseca, A. F.***; Sousa, A. G.; **Galvao, D. S.***

Recently, a new 2D carbon allotrope structure, named phagraphene (PG), was proposed. PG has a densely array of penta-hexa-hepta-graphene carbon rings. PG was shown to present low and anisotropic thermal conductivity and it is believed that this anisotropy should be also reflected in its mechanical properties. Although PG mechanical properties have been investigated, a detailed and comprehensive study is still lacking. In the present work we have carried out fully atomistic reactive molecular dynamics simulations using the ReaxFF force field, to investigate the mechanical properties and fracture patterns of PG membranes.

The Young's modulus values of the PG membranes were estimated from the stress-strain curves. Our results show that these curves present three distinct regimes: one regime where ripples dominate the structure and mechanical properties of the PG membranes; an elastic regime where the membranes exhibit fully planar configurations; and finally am inelastic regime where permanent defamations happened to the PG membrane up to the mechanical failure or fracture.

MRS ADVANCES 3[1-2], 67-72, 2018. DOI: 10.1557/adv.2018.54

[P136-2018] "Mechanical Properties of Schwarzites - A Fully Atomistic Reactive Molecular Dynamics Investigation"

Woellner, C. F.*; Botari, T.*; Perim, E.*; Galvao, D. S.*

Schwarzites are crystalline, 3D porous structures with a stable negative curvature formed of sp2-hybridized carbon atoms. These structures present topologies with tunable porous size and shape and unusual mechanical properties. In this work, we have investigated the mechanical behavior under compressive strain and energy absorption of four different Schwarzites. We considered two Schwarzites families, the so-called Gyroid and Primitive and two structures from each family. We carried out reactive molecular dynamics simulations, using the ReaxFF force field as available in the LAMMPS code. Our results also show they exhibit remarkable resilience under mechanical compression. They can be reduced to half of their original size before structural failure (fracture) occurs.

MRS ADVANCES 3[8-9], 448-453, 2018. DOI: 10.1557/adv.2018.124

[P137-2018] "Mechanical Properties of Ultralow Density Graphene Oxide/Polydimethylsiloxane Foams"

Woellner, C. F.*; Owuor, P. S.; Li, T.; Vinod, S.; Ozden, S.; Kosolwattana, S.; Bhowmick, S.; Duy, L. X.; Salvatierra, R. V.; Wei, B. Q.; Amanulla, S. A. S.; Tour, J. M.; Vajtai, R.; Lou, J.; **Galvao, D. S.***; Tiwary, C. S.; Ajayan, P. M.

Low-density, highly porous graphene/graphene oxide (GO) based-foams have shown high performance in energy absorption applications, even under high compressive deformations. In general, foams are very effective as energy dissipative materials and have been widely used in many areas such as automotive, aerospace and biomedical industries. In the case of graphene-based foams, the good mechanical properties are mainly attributed to the intrinsic graphene and/or GO electronic and mechanical properties. Despite the attractive physical properties of graphene/GO based-foams, their structural and thermal stabilities are still a problem for some applications. For instance, they are easily degraded when placed in flowing solutions, either by the collapsing of their layers or just by structural disintegration into small pieces. Recently, a new and scalable synthetic approach to produce low-density 3D macroscopic GO structure interconnected with polydimethylsiloxane (PDMS) polymeric chains (pGO) was proposed. A controlled amount of PDMS is infused into the freeze-dried foam resulting into a very rigid structure with improved mechanical properties, such as tensile plasticity and toughness. The PDMS wets the graphene oxide sheets and acts like a glue bonding PDMS and GO sheets. In order to obtain further insights on mechanisms behind the enhanced mechanical pGO response we carried out fully atomistic molecular dynamics (MD) simulations. Based on MD results, we build up a structural model that can explain the experimentally observed mechanical behavior.

MRS ADVANCES 3[1-2], 61-66, 2018. DOI: 10.1557/adv.2018.49

[P138-2018] "Mid-infrared frequency comb generation via cascaded quadratic nonlinearities in quasi-phase-matched waveguides"

Kowligy, A. S.; Lind, A.; Hickstein, D. D.; Carlson, D. R.; Timmers, H.; Nader, N.; **Cruz, F. C.***; Ycas, G.; Papp, S. B.; Diddams, S. A.

We experimentally demonstrate a simple configuration for mid-infrared (MIR) frequency comb generation in quasi-phase-matched lithium niobate waveguides using the cascaded--chi((2)) nonlinearity. With nanojoule-scale pulses from an Er: fiber laser, we observe octave-spanning supercontinuum in the near-infrared with dispersive wave generation in the 2.5-3 mu m region and intrapulse difference frequency generation in the 4-5 mu m region. By engineering the quasi-phase-matched grating profiles, tunable, narrowband MIR and broadband MIR spectra are both observed in this geometry. Finally, we perform numerical modeling using a nonlinear envelope equation, which shows good quantitative agreement with the experiment--and can be used to inform waveguide designs to tailor the MIR frequency combs. Our results identify a path to a simple single--branch approach to mid-infrared frequency comb generation in a compact platform using commercial Er: fiber technology.

OPTICS LETTERS 43[8], 1678-1681, 2018. DOI: 10.1364/OL.43.001678

[P139-2018] "Molecular dynamics simulations of ballistic penetration of penta-graphene sheets"

Azevedo, D. L.*; Bizao, R. A.*; Galvao, D. S.*

The search for new materials with low density and superior mechanical properties is a very intense and stimulating investigation area. These new materials could provide potential application for ballistic protection. Recent experiments and simulations revealed graphene possesses exceptional energy absorption properties. In this work, we analysed through fully atomistic molecular dynamics simulations the ballistic performance of a carbon-based material recently proposed named penta-graphene. Our results show that the fracture pattern is more spherical (no petals formation like observed for graphene). The estimated penetration energy for single--layer pentagraphene structures obtained here was d(1penta) similar to 37.7 MJ/kg, and is comparable with recently results obtained for graphene: d(1graphene) similar to 29.0 MJ/kg and d(1graphene) similar to 40.8 MJ/kg under similar conditions. These preliminary results are suggestive that penta-graphene could be an excellent material for ballistic applications.

MRS ADVANCES 3[8-9], 431-435, 2018. DOI: 10.1557/adv.2018.61

[P140-2018] "Morphology controlled graphene-alloy nanoparticle hybrids with tunable carbon monoxide conversion to carbon dioxide"

Devi, M. M.; Dolai, N.; Sreehala, S.; **Jaques, Y. M.***; Mishra, R. S. K.; **Galvao, D. S.***; Tiwary, C. S.; Sharma, S.; Biswas, K.

Selective oxidation of CO to CO2 using metallic or alloy nanoparticles as catalysts can solve two major problems of energy requirements and environmental pollution. Achieving 100% conversion efficiency at a lower temperature is a very important goal. This requires sustained efforts to design and develop novel supported catalysts containing alloy nanoparticles. In this regard, the decoration of nanoalloys with graphene, as a support for the catalyst, can provide a novel structure due to the synergic effect of the nanoalloys and graphene. Here, we demonstrate the effect of nano-PdPt (Palladium-Platinum) alloys having different morphologies on the catalytic efficiency for the selective oxidation of CO.

Efforts were made to prepare different morphologies of PdPt alloy nanoparticles with the advantage of tuning the capping agent (PVP - polyvinyl pyrollidone) and decorating them on graphene sheets via the wet-chemical route. The catalytic activity of the G-PdPt hybrids with an urchin--like morphology has been found to be superior (higher % conversion at 135 degrees C lower) to that with a nanoflower morphology. The above experimental observations are further supported by molecular dynamics (MD) simulations.

NANOSCALE 10[18], 8840-8850, 2018. DOI: 10.1039/c7nr09688g

[P141-2018] "New limits on neutrino magnetic moment through nonvanishing 13-mixing"

Guzzo, M. M.*; de Holanda, P. C.*; Peres, O. L. G.*

The relatively large value of the neutrino mixing angle theta(13) set by recent measurements allows us to use solar neutrinos to set a limit on the neutrino magnetic moment involving the second and third flavor families, mu(23). The existence of a random magnetic field in the solar convective zone can produce a significant antineutrino flux when a nonvanishing neutrino magnetic moment is assumed. Even if we consider a vanishing neutrino magnetic moment involving the first family, electron antineutrinos are indirectly produced through the mixing between the first and third families and mu(23)not equal 0. Using KamLAND limits on the solar flux of electron antineutrino, we set the limit mu(23) < 0.95 x 10(-1)(1)mu(B)as a reasonable assumption on the behavior of solar magnetic fields. This is the first time that a limit on mu(23) has been established in the literature directly from neutrino interactions with magnetic fields, and, interestingly enough, is comparable with the limits on the neutrino magnetic moment involving the first family and with the ones coming from modifications to the electroweak cross section.

PHYSICAL REVIEW D 97[9], 093006, 2018. DOI: 10.1103/PhysRevD.97.093006

[P142-2018] "Observation of magnetic-field-induced transitions in the DyNi3Ga9 intermetallic compound"

Mendonca, E. C.; Mercena, S. G.; Meneses, C. T.; Silva, L. S.; **Jesus, C. B. R.*; Duque, J. G. S.*; Pagliuso, P. G.***

In this work, field and temperature-dependent magnetization and specific heat measurements carried out on the DyNi3Ga9 intermetallic compound grown by Ga self-flux method are reported. This material crystallizes in a trigonal ErNi3Al9--type crystal structure with space group R32. In our previous work, we have shown that the DyNi3Ga9 compound, which orders antiferromagnetically at T-N = 10.1 K presents strong crystalline electric field (CEF) effects. At H = 1 kOe, the low--T dependence of magnetic susceptibility (T < 30 K) presents a complex behavior. For increasing applied magnetic field, a trivial antiferromagnetic-paramagnetic transition is observed. However, M(H) curves measured at selected temperatures for the magnetic field applied in the ab-plane show multiples transitions suggesting possible spin reorientations. Besides, for the low field M(H) loops one can observe the presence of coercivity, remanence and saturation effects evidencing the complex magnetic ordered state of this compound. Finally, specific heat measurements as a function of applied magnetic field show the emergence of a second peak suggesting the presence of field-induced transitions for H > 15 kOe.

INTERMETALLICS 97, 85-88, 2018. DOI: 10.1016/j.intermet.2018.03.013

[P143-2018] "Observation of the Higgs boson decay to a pair of tau leptons with the CMS detector"

Sirunyan, A. M.; Tumasyan, A.; Adam, W.; **Chinellato, J. A.*; Tonelli Manganote, E. J.***; et al.
CMS Collaboration

A measurement of the H -> tau tau signal strength is performed using events recorded in proton-proton collisions by the CMS experiment at the LHC in 2016 at a center-of-mass energy of 13TeV. The data set corresponds to an integrated luminosity of 35.9 fb(-1). The H -> tau tau signal is established with a significance of 4.9 standard deviations, to be compared to an expected significance of 4.7 standard deviations. The best fit of the product of the observed H -> tau tau signal production cross section and branching fraction is 1.09(-0.2)(6+0.27) times the standard model expectation. The combination with the corresponding measurement performed with data collected by the CMS experiment at center-of-mass energies of 7 and 8 TeV leads to an observed significance of 5.9 standard deviations, equal to the expected significance. This is the first observation of Higgs boson decays to tau leptons by a single experiment.

PHYSICS LETTERS B 779, 283-316, 2018. DOI: 10.1016/j.physletb.2018.02.004

[P144-2018] "On the Effect of Aluminum on the Microstructure and Mechanical Properties of CrN Coatings deposited by HiPIMS"

Guimaraes, M. C. R.; de Castilho, B. C. N. M.; Cunha, C.; Correr, W. R.; Mordente, P.; **Alvarez, F.***; Pinto, H. C.

Hard coatings are a suitable solution for increasing the lifetime of tools and components employed in different industrial applications. Coatings of transition metal nitrides have great use for tribological applications due to due to their unique mechanical properties. Although widely employed, current deposition methods such as cathodic arc evaporation produce coatings with many defects, which in turn reduce the resistance to wear, especially under severe conditions. High Power Impulse Magnetron Sputtering is a novel physical vapor deposition technique that produces homogeneous coatings. In this study, CrN and CrAlN monolayer coatings were deposited on AISI 304 stainless steel substrates using HiPIMS. X-Ray Diffraction, Scanning Electron Microscopy, Atomic Force Microscopy were used to evaluate the microstructure, phase composition, morphology and chemical composition of the coating. Results showed that HiPIMS is a promising technique to deposit CrN and CrAlN homogeneous coatings with high hardness and good adhesion to the substrate.

MATERIALS RESEARCH-IBERO-AMERICAN JOURNAL OF MATERIALS 21[3], UNSP e20170848, 2018. DOI: 10.1590/1980-5373-MR-2017-0848

[P145-2018] "On the effect of substrate oscillation on CrN coatings deposited by HiPIMS and dcMS"

Guimaraes, M. C. R.; de Castilho, B. C. N. M.; Nossa, T. D.; Avila, P. R. T.; **Cucatti, S.*; Alvarez, F.***; Garcia, J. L.; Pinto, H. C.

There are plenty of deposition techniques to produce hard coatings. Among them, Direct Current Magnetron Sputtering (dcMS) and High Power Impulse Magnetron Sputtering (HiPIMS) are known to produce dense coatings with few or no growth defects. Transition metal nitrides are widely used for tribological applications. CrN has been described as a high hardness, high wear resistant coating therefore making an ideal candidate to be deposited by sputtering. Although the use of multilayers have been described as a mean to further increase wear resistance, no study has presented the effect of a multilayer produced by the oscillation of the substrate during the deposition process.

This paper presents a study of the effect of the oscillation on the production of these multilayer and its effects on the mechanical and structural properties of the coating. Furthermore, the effects of bias and frequency on these properties were evaluated. To characterize the coatings it was used XRD, SEM, AFM, Nanohardness and Corrosion tests. The XRD results showed higher texture on (311) plane for -60 V for HiPIMS deposition for all frequencies leading to higher hardness. Compressive residual stresses were found to grow as the bias increased for HiPIMS deposition, whereas dcMS led to the opposite behavior. Finally, dcMS coatings presented similar corrosion resistance when compared to HiPIMS coatings.

SURFACE & COATINGS TECHNOLOGY 340, 112-120, 2018. DOI: 10.1016/j.surfcoat.2018.02.028

[P146-2018] "Optimizing power oscillations in an ellipsometric system"

Araujo, M. P.*; De Leo, S.; **Maia, G. G.***

Ellipsometry is a powerful and well-established optical technique used in the characterization of materials. It works by combining the components of elliptically polarized light in order to draw information about the optical system. We propose an ellipsometric experimental set-up to study polarization interference in the total internal reflection regime for Gaussian laser beams. The relative phase between orthogonal states can be measured as a power oscillation of the optical beam transmitted through a dielectric block, and the orthogonal components are then mixed by a polarizer. We show under which conditions the plane wave analysis is valid, and when the power oscillation can be optimized to reproduce a full pattern of oscillation and to simulate quarter- and half-wave plates.

CHINESE OPTICS LETTERS 16[3], 031406, 2018. DOI: 10.3788/COL201816.031406

[P147-2018] "Phase coexistence and magnetic behavior in the low-dimensional hexagonal cobaltites Ba(x)A(1-x)CoO(3--delta) (A = Mg or Ca and 0 <= x <= 0.20)"

Oliveira, M. P.; Mercena, S. G.; Meneses, C. T.; **Jesus, C. B. R.*; Pagliuso, P. G.*; Duque, J. G. S.***

In this work, we report on X-ray diffraction and magnetization measurements carried out in the low-dimensional hexagonal cobaltites Ba(x)A(1-x)CoO(3-delta) (A = Mg or Ca, 0 <= x <= 0.20 and delta = 0 or 0.4). Polycrystalline samples have been synthesized by solid-state reaction. The Rietveld refinements of the X-ray diffraction patterns show clearly a phase coexistence of both BaCoO2.6 and BaCoO3 hexagonal polytype structures (space group: P63/ mmc), which is dependent on both the dopant ion and doping level. At low temperatures (T < 50 K), the ZFC-FC data recorded at H = 1 kOe for Ca-doped (x < 0.15) and Ba0.80Mg0.20CoO3-delta samples present a broad peak and strong thermal hysteresis. Besides, a second anomaly around room temperature is also observed in susceptibility curves for all samples. Further increasing in the Ca-doping produces a continuous decreasing of magnetization and for the samples with x > 0.10 the low temperature hysteresis is not observed anymore. The field-dependence of ZFC-FC curves taken for the sample grown with x = 0 show a displacement of the peak position into low temperature region. Except for the sample grown with x = 0.20, the MvsH loops taken at T = 2 K show multiple steps in the field region ranging -15 <= H <= 15 kOe. Finally, the saturation magnetization values are consistent with a low-spin state for the Co2+ or Co4+ ions.

JOURNAL OF MAGNETISM AND MAGNETIC MATERIALS 451, 774-779, 2018. DOI: 10.1016/j.jmmm.2017.12.020

[P148-2018] "Phase equilibrium and physical properties of biobased ionic liquid mixtures"

Hijo, A. A. C. T.; Maximo, G. J.; Cunha, R. L.; **Fonseca, F. H. S.*; Cardoso, L. P.***; Pereira, J. F. B.; Costa, M. C.; Batista, E. A. C.; Meirelles, A. J. A.

Protic ionic liquid crystals (PILCs) obtained from natural sources are promising compounds due to their peculiar properties and sustainable appeal. However, obtaining PILCs with higher thermal and mechanical stabilities for product and process design is in demand and studies on such approaches using this new IL generation are still scarce. In this context, this work discloses an alternative way for tuning the physicochemical properties of ILCs by mixing PILs. New binary mixtures of PILs derived from fatty acids and 2-hydroxy ethylamines have been synthesized here and investigated through the characterization of the solid-solid-[liquid crystal]-liquid thermodynamic equilibrium and their rheological and critical micellar concentration profiles. The mixtures presented a marked nonideal melting profile with the formation of solid solutions. This work revealed an improvement of the PILCs' properties based on a significant increase in the ILC temperature domain and the obtainment of more stable mesophases at high temperatures when compared to pure PILs. In addition, mixtures of PILs also showed significant changes in their non-Newtonian and viscosity profile up to 100 s(-1), as well as mechanical stability over a wide temperature range. The enhancement of the physicochemical properties of PILs here disclosed by such an approach leads to more new possibilities of their industrial application at high temperatures.

PHYSICAL CHEMISTRY CHEMICAL PHYSICS 20[9], 6469-6479, 20185. DOI: 10.1039/c7cp06841g

[P149-2018] "pi(0) and eta meson production in proton-proton collisions at root s=8 TeV"

Acharya, S.; Adam, J.; Adamova, D.; **Albuquerque, D. S. D.*; Chinellato, D. D.*; De Souza, R. D.*; Takahashi, J.***; et al. ALICE Collaboration

An invariant differential cross section measurement of inclusive pi(0) and eta meson production atmid-rapidity in pp collisions at root s = 8 TeV was carried out by the ALICE experiment at the LHC. The spectra of pi(0) and eta mesons were measured in transverse momentum ranges of 0.3 < p(T) < 35 GeV/c and 0.5 < p(T) < 35 GeV/c, respectively. Next-to-leading order perturbative QCD calculations using fragmentation functions DSS14 for the pi(0) and AESSS for the. overestimate the cross sections of both neutral mesons, although such calculations agree with the measured eta/pi(0) ratio within uncertainties. The results were also compared with PYTHIA 8.2 predictions for which the Monash 2013 tune yields the best agreement with the measured neutral meson spectra. The measurements confirm a universal behavior of the eta/pi(0) ratio seen forNA27, PHENIX and ALICE data for pp collisions from root s = 27.5 GeV to root s = 8 TeV within experimental uncertainties. A relation between the pi(0) and eta production cross sections for pp collisions at root s = 8 TeV is given by m(T) scaling for p(T) > 3.5 GeV/c. However, a deviation from this empirical scaling rule is observed for transverse momenta below p(T) < 3.5 GeV/c in the eta/pi(0) ratio with a significance of 6.2 sigma.

EUROPEAN PHYSICAL JOURNAL C 78[3], 263, 2018. DOI: 10.1140/epjc/s10052-018-5612-8

[P150-2018] "Production of He-4 and (4)<(He) over bar> in Pb-Pb collisions at root(NN)-N-S=2.76 TeV at the LHC"

Acharya, S.; Adamova, D.; Adolfsson, J.; **Albuquerque, D. S. D.*; Chinellato, D. D.*; De Souza, R. D.*; Takahashi, J.***; et al.

Results on the production of He-4 and (4)<(He) over bar> nuclei in Pb-Pb collisions at root(NN)-N-S = 2.76 TeV in the rapidity range vertical bar y vertical bar < 1, using the ALICE detector, are presented in this paper. The rapidity densities corresponding to 0-10% central events are found to be dN/dy4(He) = (0.8 +/- 0.4 (stat) +/- 0.3 (syst)) x 10(-6) and dN/dy4<(He) over bar> = (1.1 +/- 0.4 (stat) +/- 0.2 (syst)) x 10(-6), respectively. This is in agreement with the statistical thermal model expectation assuming the same chemical freeze-out temperature (T-chem = 156 MeV) as for light hadrons. The measured ratio of (4)<(He) over bar>/He-4 is 1.4 +/- 0.8 (stat) +/- 0.5 (syst).

NUCLEAR PHYSICS A 971, 1-20, 2018. DOI: 10.1016/j.nuclphysa.2017.12.004

[P151-2018] "Proximity effects in chromosome aberration induction: Dependence on radiation quality, cell type and dose"

Cajiao, J. J. T.*; Carante, M. P.; **Bernal, M. A.***; Ballarini, F.

It is widely accepted that, in chromosome-aberration induction, the (mis-)rejoining probability of two chromosome fragments depends on their initial distance, r. However, several aspects of these "proximity effects" need to be clarified, also considering that they can vary with radiation quality, cell type and dose. A previous work performed by the BIANCA (Biophysical ANalysis of Cell death and chromosome Aberrations) biophysical model has suggested that, in human lymphocytes and fibroblasts exposed to low-LET radiation, an exponential function of the form exp(-r/r(0)), which is consistent with free-end (confined) diffusion, describes proximity effects better than a Gaussian function. Herein, the investigation was extended to intermediate- and high-LET. Since the 41 values (0.8 mu m for lymphocytes and 0.7 mu m for fibroblasts) were taken from the low-LET study, the results were obtained by adjusting only one model parameter, i.e. the yield of "Cluster Lesions" (CLs), where a CL was defined as a critical DNA damage producing two independent chromosome fragments. In lymphocytes, the exponential model allowed reproducing both dose-response curves for different aberrations (dicentrics, centric rings and excess acentrics), and values of F-ratio (dicentrics to centric rings) and G-ratio (interstitial deletions to centric rings). In fibroblasts, a good correspondence was found with the dose-response curves, whereas the G-ratio (and, to a lesser extent, the F-ratio) was underestimated. With increasing LET, F decreased and G increased in both cell types, supporting their role as "fingerprints" of high-LET exposure. A dose-dependence was also found at high LET, where F increased with dose and G decreased, possibly due to inter-track effects. We therefore conclude that, independent of radiation quality, in lymphocytes an exponential function can describe proximity effects at both inter- and intra-chromosomal level; on the contrary, in fibroblasts further studies (experimental and theoretical) are needed to explain the strong bias for intra-arm relative to inter-arm exchanges.

DNA REPAIR 64, 45-52, 2018. DOI: 10.1016/j.dnarep.2018.02.006

[P152-2018] "Revealing the nature of low-temperature photoluminescence peaks by laser treatment in van der Waals epitaxially grown WS2 monolayers"

Orsi Gordo, V.*; Balanta, M. A. G.; Gobato, Y. G.; Covre, F. S.; Galeti, H. V. A.; **Iikawa, F.*; Couto, O. D. D.***; Qu, F.; Henini, M.; Hewak, D. W.; Huang, C. C.

Monolayers of transition metal dichalcogenides (TMD) are promising materials for optoelectronics devices. However, one of the challenges is to fabricate large-scale growth of high quality TMD monolayers with the desired properties in order to expand their use in potential applications. Here, we demonstrate large-scale tungsten disulfide (WS2) monolayers grown by van der Waals Epitaxy (VdWE). We show that, in addition to the large structural uniformity and homogeneity of these samples, their optical properties are very sensitive to laser irradiation. We observe a time instability in the photoluminescence (PL) emission at low temperatures in the scale of seconds to minutes. Interestingly, this change of the PL spectra with time, which is due to laser induced carrier doping, is employed to successfully distinguish the emission of two negatively charged bright excitons. Furthermore, we also detect blinking sharp bound exciton emissions which are usually attractive for single photon sources. Our findings contribute to a deeper understanding of this complex carrier dynamics induced by laser irradiation which is very important for future optoelectronic devices based on large scale TMD monolayers.

NANOSCALE 10[10], 4807-4815, 2018. DOI: 10.1039/c8nr00719e

[P153-2018] "Scale Effects on the Ballistic Penetration of Graphene Sheets"

Bizao, R. A.*; Machado, L. D.*; de Sousa, J. M.*; Pugno, N. M.; **Galvao, D. S.***

Carbon nanostructures are promising ballistic protection materials, due to their low density and excellent mechanical properties. Recent experimental and computational investigations on the behavior of graphene under impact conditions revealed exceptional energy absorption properties as well. However, the reported numerical and experimental values differ by an order of magnitude. In this work, we combined numerical and analytical modeling to address this issue. In the numerical part, we employed reactive molecular dynamics to carry out ballistic tests on single, double, and triple-layered graphene sheets. We used velocity values within the range tested in experiments. Our numerical and the experimental results were used to determine parameters for a scaling law. We find that the specific penetration energy decreases as the number of layers (N) increases, from similar to 15 MJ/kg for N = 1 to similar to 0.9 MJ/kg for N = 350, for an impact velocity of 900 m/s. These values are in good agreement with simulations and experiments, within the entire range of N values for which data is presently available. Scale effects explain the apparent discrepancy between simulations and experiments.

SCIENTIFIC REPORTS 8, 6750, 2018. DOI: 10.1038/s41598-018-25050-2

[P154-2018] "Schwarzites for Natural Gas Storage: A Grand - Canonical Monte Carlo Study"

Borges, D. D.*; Galvao, D. S.*

The 3D porous carbon-based structures called Schwarzites have been recently a subject of renewed interest due to the possibility of being synthesized in the near future. These structures exhibit negatively curvature topologies with tuneable porous sizes and shapes, which make them natural candidates for applications such as CO2 capture, gas storage and separation. Nevertheless, the adsorption properties of these materials have not been fully investigated. Following this motivation, we have carried out Grand-Canonical Monte Carlo simulations to study the adsorption of small molecules such as CO2, CO, CH4, N-2 and H-2, in a series of Schwarzites structures. Here, we present our preliminary results on natural gas adsorptive capacity in association with analyses of the guest-host interaction strengths. Our results show that Schwarzites P7par, P8bal and IWPg are the most promising structures with very high CO2 and CH4 adsorption capacity and low saturation pressure (<1bar) at ambient temperature. The P688 is interesting for H-2 storage due to its exceptional high H-2 adsorption enthalpy value of -19kJ/mol.

MRS ADVANCES 3[1-2], 115-120, 2018. DOI: 10.1557/adv.2018.190

[P155-2018] "Search for a heavy resonance decaying to a pair of vector bosons in the lepton plus merged jet final state root s=13 TeV"

Sirunyan, A. M.; Tumasyan, A.; Adam, W.; **Chinellato, J. A.*; Tonelli Manganote, E. J.*;** et al.
CMS Collaboration

A search for a new heavy particle decaying to a pair of vector bosons (WW or WZ) is presented using data from the CMS detector corresponding to an integrated luminosity of 35.9 fb(-1) collected in proton-proton collisions at a centre-of-mass energy of 13 TeV in 2016. One of the bosons is required to be a W boson decaying to e nu or mu nu, while the other boson is required to be reconstructed as a single massive jet with substructure compatible with that of a highly-energetic quark pair from a W or Z boson decay. The search is performed in the resonance mass range between 1.0 and 4.4 TeV. The largest deviation from the background-only hypothesis is observed for a mass near 1.4 TeV and corresponds to a local significance of 2.5 standard deviations. The result is interpreted as an upper bound on the resonance production cross section. Comparing the excluded cross section values and the expectations from theoretical calculations in the bulk graviton and heavy vector triplet models, spin-2 WW resonances with mass smaller than 1.07 TeV and spin-1 WZ resonances lighter than 3.05 TeV, respectively, are excluded at 95% confidence level.

JOURNAL OF HIGH ENERGY PHYSICS [5], 088, 2018. DOI: 10.1007/JHEP05(2018)088

[P156-2018] "Search for electroweak production of charginos and neutralinos in multilepton final states in proton--proton collisions at root s=13 TeV"

Sirunyan, A. M.; Tumasyan, A.; Adam, W.; **Chinellato, J. A.*; Tonelli Manganote, E. J.***; et al.
CMS Collaboration

Results are presented from a search for the direct electroweak production of charginos and neutralinos in signatures with either two or more leptons (electrons or muons) of the same electric charge, or with three or more leptons, which can include up to two hadronically decaying tau leptons. The results are based on a sample of proton proton collision data collected at root s = 13 TeV, recorded with the CMS detector at the LHC, corresponding to an integrated luminosity of 35.9 fb(-1). The observed event yields are consistent with the expectations based on the standard model. The results are interpreted in simplified models of supersymmetry describing various scenarios for the production and decay of charginos and neutralinos. Depending on the model parameters chosen, mass values between 180 GeV and 1150 GeV are excluded at 95% CL. These results significantly extend the parameter space probed for these particles in searches at the LHC. In addition, results are presented in a form suitable for alternative theoretical interpretations.

JOURNAL OF HIGH ENERGY PHYSICS [3], 166, 2018. DOI: 10.1007/JHEP03(2018)166

[P157-2018] "Search for lepton-flavor violating decays of heavy resonances and quantum black holes to e mu final states in proton-proton collisions at root s=13 TeV"

Sirunyan, A. M.; Tumasyan, A.; Adam, W.; **Chinellato, J. A.*; Tonelli Manganote, E. J.***; et al.
CMS Collaboration

A search is reported for heavy resonances decaying into e mu final states in proton-proton collisions recorded by the CMS experiment at the CERN LHC at root s = 13 TeV, corresponding to an integrated luminosity of 35.9 fb(-1). The search focuses on resonance masses above 200 GeV. With no evidence found for physics beyond the standard model in the e mu mass spectrum, upper limits are set at 95% confidence level on the product of the cross section and branching fraction for this lepton-flavor violating signal. Based on these results, resonant tau sneutrino production in R-parity violating supersymmetric models is excluded for masses below 1.7 TeV, for couplings lambda(132) = lambda(231) = lambda(311) = 0.01. Heavy Z' gauge bosons with lepton-flavor violating transitions are excluded for masses up to 4.4 TeV. The eit mass spectrum is also interpreted in terms of non-resonant contributions from quantum black--hole production in models with one to six extra spatial dimensions, and lower mass limits are found between 3.6 and 5.6 TeV. In all interpretations used in this analysis, the results of this search improve previous limits by about 1 TeV. These limits correspond to the most sensitive values obtained at colliders.

JOURNAL OF HIGH ENERGY PHYSICS [4], 073, 2018. DOI: 10.1007/JHEP04(2018)073

[P158-2018] "Search for massive resonances decaying into WW, WZ, ZZ, qW, and qZ with dijet final states at root s=13 TeV"

Sirunyan, A. M.; Tumasyan, A.; Adam, W.; **Chinellato, J. A.*; Tonelli Manganote, E. J.***; et al.
CMS Collaboration

Results are presented from a search in the dijet final state for new massive narrow resonances decaying to pairs of W and Z bosons or to a W/Z boson and a quark. Results are based on data recorded in proton-proton collisions at root s = 13 TeV with the CMS detector at the CERN LHC. The data correspond to an integrated luminosity of 35.9 fb(-1). The mass range investigated extends upwards from 1.2 TeV. No excess is observed above the estimated standard model background and limits are set at 95% confidence level on cross sections, which are interpreted in terms of various models that predict gravitons, heavy spin-1 bosons, and excited quarks. In a heavy vector triplet model, W' and Z' resonances, with masses below 3.2 and 2.7 TeV, respectively, and spin-1 resonances with degenerate masses below 3.8 TeV are excluded at 95% confidence level. In the case of a singlet W' resonance masses between 3.3 and 3.6 TeV can be excluded additionally. Similarly, excited quark resonances, q*, decaying to qW and qZ with masses less than 5.0 and 4.7 TeV, respectively, are excluded. In a narrow-width bulk graviton model, upper limits are set on cross sections ranging from 0.6 fb for high resonance masses above 3.6 TeV, to 36.0 fb for low resonance masses of 1.3 TeV.

PHYSICAL REVIEW D 97[7], 072006, 2017. DOI: 10.1103/PhysRevD.97.072006

[P159-2018] "Search for Narrow Resonances in the b-Tagged Dijet Mass Spectrum in Proton-Proton Collisions at root s=8 TeV"

Sirunyan, A. M.; Tumasyan, A.; Adam, W.; **Chinellato, J. A.*; Tonelli Manganote, E. J.***; et al.
CMS Collaboration

A search for narrow resonances decaying to bottom quark--antiquark pairs is presented, using a data sample of proton--proton collisions at root s = 8 TeV corresponding to an integrated luminosity of 19.7 fb(-1). The search is extended to masses lower than those reached in typical searches for resonances decaying into jet pairs at the LHC, by taking advantage of triggers that identify jets originating from bottom quarks.

No significant excess of events is observed above the background predictions. Limits are set on the product of cross section and branching fraction to bottom quarks for spin 0, 1, and 2 resonances in the mass range of 325-1200 GeV. These results improve on the limits for resonances decaying into jet pairs in the 325-500 GeV mass range.

PHYSICAL REVIEW LETTERS 120[20], 201801, 2018. DOI: 10.1103/PhysRevLett.120.201801

[P160-2018] "Search for natural and split supersymmetry in proton-proton collisions at root s=13 TeV in final states with jets and missing transverse momentum"

Sirunyan, A. M.; Tumasyan, A.; Adam, W.; **Chinellato, J. A.*; Tonelli Manganote, E. J.***; et al.
CMS Collaboration

A search for supersymmetry (SUSY) is performed in final states comprising one or more jets and missing transverse momentum using data from proton-proton collisions at a centre-of--mass energy of 13 TeV. The data were recorded with the CMS detector at the CERN LHC in 2016 and correspond to an integrated luminosity of 35.9 fb(-1). The number of signal events is found to agree with the expected background yields from standard model processes. The results are interpreted in the context of simplified models of SUSY that assume the production of gluino or squark pairs and their prompt decay to quarks and the lightest neutralino. The masses of bottom, top, and mass-degenerate light-flavour squarks are probed up to 1050, 1000, and 1325 GeV, respectively. The gluino mass is probed up to 1900, 1650, and 1650 GeV when the gluino decays via virtual states of the aforementioned squarks. The strongest mass bounds on the neutralinos from gluino and squark decays are 1150 and 575 GeV, respectively. The search also provides sensitivity to simplified models inspired by split SUSY that involve the production and decay of long-lived gluinos. Values of the proper decay length CT0 from 10(-3) to 10(5) mm are considered, as well as a metastable gluino scenario. Gluino masses up to 1750 and 900 GeV are probed for CT0 = 1mm and for the metastable state, respectively. The sensitivity is moderately dependent on model assumptions for CT0 greater than or similar to 1 m. The search provides coverage of the CT0 parameter space for models involving long-lived gluinos that is complementary to existing techniques at the LHC.

JOURNAL OF HIGH ENERGY PHYSICS [5], 025, 2018. DOI: 10.1007/JHEP05(2018)025

[P161-2018] "Search for natural supersymmetry in events with top quark pairs and photons in pp collisions at root s=8 TeV"

Sirunyan, A. M.; Tumasyan, A.; Adam, W.; **Chinellato, J. A.*; Tonelli Manganote, E. J.***; et al.
CMS Collaboration

Results are presented from a search for natural gauge-mediated supersymmetry (SUSY) in a scenario in which the top squark is the lightest squark, the next-to-lightest SUSY particle is a bino--like neutralino, and the lightest SUSY particle is the gravitino. The strong production of top squark pairs can produce events with pairs of top quarks and neutralinos, with each bino-like neutralino decaying to a photon and a gravitino. The search is performed using a sample of pp collision data accumulated by the CMS experiment at root s = 8 TeV, corresponding to an integrated luminosity of 19.7 fb(-1). The final state consists of a lepton (electron or muon), jets, and one or two photons. The imbalance in transverse momentum in the events is compared with the expected spectrum from standard model processes. No excess event yield is observed beyond the expected background, and the result is interpreted in the context of a general model of gauge-mediated SUSY breaking that leads to exclusion of top squark masses below 650-730 GeV.

JOURNAL OF HIGH ENERGY PHYSICS [3], 167, 2018. DOI: 10.1007/JHEP03(2018)167

[P162-2018] "Search for new phenomena in final states with two opposite-charge, same-flavor leptons, jets, and missing transverse momentum in pp collisions at root s=13TeV"

Sirunyan, A. M.; Tumasyan, A.; Adam, W.; **Chinellato, J. A.*; Tonelli Manganote, E. J.***; et al.
CMS Collaboration

Search results are presented for physics beyond the standard model in final states with two opposite-charge, same-flavor leptons, jets, and missing transverse momentum. The data sample corresponds to an integrated luminosity of 35.9 fb(-1) of proton-proton collisions at root s = 13TeV collected with the CMS detector at the LHC in 2016. The analysis uses the invariant mass of the lepton pair, searching for a kinematic edge or a resonant-like excess compatible with the Z boson mass. The search for a kinematic edge targets production of particles sensitive to the strong force, while the resonance search targets both strongly and electroweakly produced new physics. The observed yields are consistent with the expectations from the standard model, and the results are interpreted in the context of simplified models of supersymmetry. In a gauge mediated supersymmetry breaking (GMSB) model of gluino pair production with decay chains including Z bosons, gluino masses up to 1500-1770 GeV are excluded at the 95% confidence level depending on the lightest neutralino mass. In a model of electroweak chargino-neutralino production, chargino masses as high as 610 GeV are excluded when the lightest neutralino is massless. In GMSB models of electroweak neutralino-neutralino production, neutralino masses up to 500-650 GeV are excluded depending on the decay mode assumed. Finally, in a model with bottom squark pair production and decay chains resulting in a kinematic edge in the dilepton invariant mass distribution, bottom squark masses up to 980-1200 GeV are excluded depending on the mass of the next-to-lightest neutralino.

JOURNAL OF HIGH ENERGY PHYSICS [3], 076, 2018. DOI: 10.1007/JHEP03(2018)076

[P163-2018] "Search for new physics in events with a leptonically decaying Z boson and a large transverse momentum imbalance in proton-proton collisions at root s=13 TeV"

Sirunyan, A. M.; Tumasyan, A.; Adam, W.; **Chinellato, J. A.*; Tonelli Manganote, E. J.***; et al.
CMS Collaboration

A search for new physics in events with a Z boson produced in association with large missing transverse momentum at the LHC is presented. The search is based on the 2016 data sample of proton-proton collisions recorded with the CMS experiment at root s = 13 TeV, corresponding to an integrated luminosity of 35.9 fb(-1). The results of this search are interpreted in terms of a simplified model of dark matter production via spin-0 or spin-1 mediators, a scenario with a standard-model--like Higgs boson produced in association with the Z boson and decaying invisibly, a model of unparticle production, and a model with large extra spatial dimensions. No significant deviations from the background expectations are found, and limits are set on relevant model parameters, significantly extending the results previously achieved in this channel.

EUROPEAN PHYSICAL JOURNAL C 78[4], 291, 2018. DOI: 10.1140/epjc/s10052-018-5740-1

[P164-2018] "Search for pair production of vector-like quarks in the bW(b)over-barW channel from proton-proton collisions at root s=13TeV"

Sirunyan, A. M.; Tumasyan, A.; Adam, W.; **Chinellato, J. A.*; Tonelli Manganote, E. J.***; et al.
CMS Collaboration

A search is presented for the production of vector-like quark pairs, T (T) over bar or Y (Y) over bar, with electric charge of 2/3(T) or -4/3(Y), in proton-proton collisions at root s= 13 TeV. The data were collected by the CMS experiment at the LHC in 2016 and correspond to an integrated luminosity of 35.8 fb(-1). The T and Y quarks are assumed to decay exclusively to a W boson and a b quark. The search is based on events with a single isolated electron or muon, large missing transverse momentum, and at least four jets with large transverse momenta. In the search, a kinematic reconstruction of the final state observables is performed, which would permit a signal to be detected as a narrow mass peak (approximate to 7% resolution). The observed number of events is consistent with the standard model prediction. Assuming strong pair production of the vector-like quarks and a 100% branching fraction to bW, a lower limit of 1295 GeV at 95% confidence level is set on the T and Y quark masses.

PHYSICS LETTERS B 779, 82-106, 2018. DOI: 10.1016/j.physletb.2018.01.077

[P165-2018] "Search for supersymmetry with Higgs boson to diphoton decays using the razor variables at root s=13 TeV"

Sirunyan, A. M.; Tumasyan, A.; Adam, W.; **Chinellato, J. A.*; Tonelli Manganote, E. J.***; et al.
CMS Collaboration

An inclusive search for anomalous Higgs boson production in the diphoton decay channel and in association with at least one jet is presented, using LHC proton-proton collision data collected by the CMS experiment at a center-of-mass energy of 13 TeV and corresponding to an integrated luminosity of 35.9 fb(-1). The razor variables M-R and R-2, as well as the momentum and mass resolution of the diphoton system, are used to categorize events into different search regions. The search result is interpreted in the context of strong and electroweak production of supersymmetric particles. We exclude bottom squark pair-production with masses below 450 GeV for bottom squarks decaying to a bottom quark, a Higgs boson, and the lightest supersymmetric particle (LSP) for LSP masses below 250 GeV. For wino-like chargino-neutralino production, we exclude charginos with mass below 170 GeV for LSP masses below 25 GeV. In the GMSB scenario, we exclude charginos with mass below 205 GeV for neutralinos decaying to a Higgs boson and a goldstino LSP with 100% branching fraction.

PHYSICS LETTERS B 779, 166-190, 2018. DOI: 10.1016/j.physletb.2017.12.069

[P166-2018] "Search for the X(5568) State Decaying into B-s(0)pi(+/-) in Proton-Proton Collisions at root s=8 TeV"

Sirunyan, A. M.; Tumasyan, A.; Adam, W.; **Chinellato, J. A.*; Tonelli Manganote, E. J.***; et al.
CMS Collaboration

A search for resonancelike structures in the B-s(0)pi(+/-) invariant mass spectrum is performed using proton-proton collision data collected by the CMS experiment at the LHC at root s = 8 TeV, corresponding to an integrated luminosity of 19.7 fb(-1). The B-s(0) mesons are reconstructed in the decay chain B-s(0) -> J/Psi phi, with J/Psi -> mu(+) mu(-) and phi -> K+K-. The B-s(0)pi(+/-) invariant mass distribution shows no statistically significant peaks for different selection requirements on the reconstructed B-s(0) and pi(+/-) candidates. Upper limits are set on the relative production rates of the X(5568) and B-s(0) states times the branching fraction of the decay X(5568)(+/-) -> B-s(0)pi(+/-). In addition, upper limits are obtained as a function of the mass and the natural width of possible exotic states decaying into B-s(0)pi(+/-).

PHYSICAL REVIEW LETTERS 120[20], 202005, 2018. DOI: 10.1103/PhysRevLett.120.202005

[P167-2018] "Search for vectorlike light-flavor quark partners in proton-proton collisions at root s=8 TeV"

Sirunyan, A. M.; Tumasyan, A.; Adam, W.; **Chinellato, J. A.*; Tonelli Manganote, E. J.***; et al.
CMS Collaboration

A search is presented for heavy vectorlike quarks (VLQs) that couple only to light quarks in proton-proton collisions at root s = 8 TeV at the LHC. The data were collected by the CMS experiment during 2012 and correspond to an integrated luminosity of 19.7 fb(-1). Both single and pair production of VLQs are considered. The single-production search is performed for down-type VLQs (electric charge of magnitude 1/3), while the pair-production search is sensitive to up-type (charge of magnitude 2/3) and down-type VLQs. Final states with at least one muon or one electron are considered. No significant excess over standard model expectations is observed, and lower limits on the mass of VLQs are derived. The lower limits range from 400 to 1800 GeV, depending on the single--production cross section and the VLQ branching fractions B to W, Z, and Higgs bosons. When considering pair production alone, VLQs with masses below 845 GeV are excluded for B(W) = 1.0, and below 685 GeV for B(W) = 0.5, B(Z) = B(H) = 0.25. The results are more stringent than those previously obtained for single and pair production of VLQs coupled to light quarks.

PHYSICAL REVIEW D 97[7], 072008, 2018. DOI: 10.1103/PhysRevD.97.072008

[P168-2018] "Self-Driven Graphene Tearing and Peeling: A Fully Atomistic Molecular Dynamics Investigation"

Fonseca, A. F.*; Galvao, D. S.*

In spite of years of intense research, graphene continues to produce surprising results. Recently, it was experimentally observed that under certain conditions graphene can self-drive its tearing and peeling from substrates. This process can generate long, micrometer sized, folded nanoribbons without the action of any external forces. Also, during this cracking--like propagation process, the width of the graphene folded ribbon continuously decreases and the process only stops when the width reaches about few hundreds nanometers in size. It is believed that interplay between the strain energy of folded regions, breaking of carbon-carbon covalent bonds, and adhesion of graphene-graphene and graphene-substrate are the most fundamental features of this process, although the detailed mechanisms at atomic scale remain unclear. In order to gain further insights on these processes we carried out fully atomistic reactive molecular dynamics simulations using the AIREBO potential as available in the LAMMPS computational package. Although the reported tearing/peeling experimental observations were only to micrometer sized structures, our results showed that they could also occur at nanometer scale. Our preliminary results suggest that the graphene tearing/peeling process originates from thermal energy fluctuations that results in broken bonds, followed by strain release that creates a local elastic wave that can either reinforce the process, similar to a whip cracking propagation, or undermine it by producing carbon dangling bonds that evolve to the formation of bonds between the two layers of graphene.

As the process continues in time and the folded graphene decreases in width, the carbon-carbon bonds at the ribbon edge and interlayer bonds get less stressed, thermal fluctuations become unable to break them and the process stops.

MRS ADVANCES 3[8-9], 460-465, 2018. DOI: 10.1557/adv.2018.120

[P169-2018] "Self-Sustained Laser Pulsation in Active Optomechanical Devices"

Princepe, D.*; Wiederhecker, G. S.*; Favero, I.; **Frateschi, N. C.***

We developed a model for an active optomechanical cavity embedding a semiconductor optical gain medium in the presence of dispersive and dissipative optomechanical couplings. Radiation pressure drives the mechanical oscillation and the back--action occurs due to the mechanical modulation of the cavity loss rate. Our numerical analysis utilizing this model shows that, even in a wideband gain material, such mechanism couples the mechanical vibration with the laser relaxation oscillation, enabling an effect of self-pulsed laser emission. In order to investigate this effect, we propose a bullseye-shaped device with high confinement of both the optical and the mechanical modes at the edge of a disk combined with a dissipative structure in its vicinity. The dispersive interaction is promoted by the strong photoelastic effect while the dissipative mechanism is governed by the boundary motion mechanism, enhanced by near-field interaction with the absorptive structure. This hybrid optomechanical device is shown to lead sufficient coupling for the experimental demonstration of the self-pulsed emission.

IEEE PHOTONICS JOURNAL 10[3], 4500610, 2018. DOI: 10.1109/JPHOT.2018.2831001

[P170-2018] "Shift of zero-dispersion wavelength in bent optical fibers"

Gil-Molina, A.*; Perez-Ramirez, A.*; Ramirez, J. C.; Gabrielli, L. H.; **Fragnito, H. L.***

The understanding of how bending modifies the dispersion of optical fibers, in particular, the zero-dispersion wavelength (lambda(0)), is essential in the development of compact nonlinear optical devices such as parametric amplifiers, wavelength converters, soliton lasers and frequency comb generators. Typically, substantial variations in the parametric gain and/or conversion efficiency are significant for changes in lambda(0) of similar to 0.1 nm, which occur for variations on the bending radius (R-b) of 1 cm or less. Measuring lambda(0) as a function of bending radius (R-b) is challenging, as it requires detecting changes < 0.1 nm and in short fibers. By using a method based on four-wave mixing (FWM) generated by an incoherent-pump with relatively broad spectrum and a weak laser, we report measurements of lambda(0) as a function of Rb in a dispersion-shifted fiber with <0.1 nm accuracy on lambda(0). This method is sensitive enough to measure small variations in lambda(0) of similar to 0.04 nm in very short fibers (similar to 20 m). We observe that lambda(0) increases by 12 nm when R-b is decreased from 10 cm to 1 cm, and a change of 1 nm is obtained for R-b = 3 cm. We also present numerical simulations of the bent fiber that are in good agreement with our measurements, and help us to explain the observations and to predict how high-order dispersion is modified with bending. This study can provide insights for dispersion engineering, in which bending could be used as a tuning, equalization, or tailoring mechanism for lambda(0), which can be used in the development of compact nonlinear optical devices based on fibers or other bent-waveguide structures.

OPTICS EXPRESS 26[6], 6700-6714, 2018. DOI: 10.1364/OE.26.006700

[P171-2018] "Silver Hardening via Hypersonic Impacts"

Oliveira, E. F.*; Autreto, P. A. D.*; Galvao, D. S.*

The search for new ultra strong materials has been a very active research area. With relation to metals, a successful way to improve their strength is by the creation of a gradient of nanograins (GNG) inside the material. Recently, R. Thevamaran et al. [Science v354, 312-316 (2016)] propose a single step method based on high velocity impact of silver nanocubes to produce high-quality GNG. This method consists of producing high impact collisions of silver cubes at hypersonic velocity (similar to 400 m/s) against a rigid wall. Although they observed an improvement in the mechanical properties of the silver after the impact, the GNG creation and the strengthening mechanism at nanoscale remain unclear. In order to gain further insights about these mechanisms, we carried out fully atomistic molecular dynamics simulations (MD) to investigate the atomic conformations/rearrangements during and after high impact collisions of silver nanocubes at ultrasonic velocity. Our results indicate the coexistence of polycrystalline arrangements after the impact formed by core HCP domains surrounded by FCC ones, which could also contribute to explain the structural hardening.

MRS ADVANCES 3[8-9], 489-494, 2018. DOI: 10.1557/adv.2018.173

[P172-2018] "Single crystal growth and characterization of the intermetallic cubic cage system YCo1.82Mn0.18Zn20"

Cabrera-Baez, M.*; Finatti, B. F.; **Rettori, C.***; Avila, M. A.

We report on the growth of YCo2-xMnxZn20 cubic single crystals (0 <= x <= 0.18) and their characterization through elemental analysis, x-ray diffraction, magnetization and heat capacity. Mn intermediate and/or mixed-valence-like behavior was observed in the magnetic response of YCo1.82Mn0.18Zn20 (and all other samples) at temperatures between 100 K and 200 K, and a spin--glass state is established at low temperatures. Specific heat results for x = 0.18 show an increased Sommerfeld coefficient of gamma approximate to 100 mJ/mol. K-2 compared to that of the undoped compound (18 mJ/mol. K-2) suggesting an enhancement of the quasiparticle effective mass ignoring spin- glass effects at very low temperatures. The combination of different experimental data provides a better understanding of the Mn2+ effects in the weakly correlated electron compound of YCo-2Zn20, the first case in this family of compounds where local magnetic moments come exclusively from the transition metal.

PHYSICA B-CONDENSED MATTER 536, 850-854, 2018. DOI: 10.1016/j.physb.2017.09.003

[P173-2018] "Six-wave mixing coherent anti-Stokes Raman scattering microscopy"

Pelegati, V. B.*; Kyotoku, B. B. C.*; Padilha, L. A.*; Cesar, C. L.*

Acquiring images of biological tissues and cells without the assistance of exogenous labels with a fast repetition rate and chemical specificity is what coherent anti-Stokes Raman Scattering (CARS) imaging offers. Nonresonant background (NRB) is one of the main drawbacks of the CARS microscopy technique because it limits the detection of weak Raman lines and the detection of low-concentration molecules. We show that a six-wave mixing process with two beams, which is a cascade effect of CARS, show better signal/NRB ratio and can be utilized for biological tissues imaging. The cascade CARS (CCARS) depends on chi-3 to the fourth power, instead of chi-3 squared as in the usual CARS signal; therefore, the contrast ratio with NRB is higher for CCARS than for CARS. We present analytic calculations showing that CCARS have better contrast over CARS in any situation.

Comparison of the signals of both techniques generated on water-ethanol solutions confirm these results. Finally, we acquired CCARS images of fresh biological tissues, attesting that it is a useful tool for biological studies.

BIOMEDICAL OPTICS EXPRESS 9[5], 2407-2417, 2018. DOI: 10.1364/BOE.9.002407

[P174-2018] "Structuration of lipid bases with fully hydrogenated crambe oil and sorbitan monostearate for obtaining zero-trans/low sat fats"

Stahl, M. A.; Buscato, M. H. M.; Grimaldi, R.; **Cardoso, L. P.***; Ribeiro, A. P. B.

Several studies have shown that excessive intake of trans and saturated fatty acids is associated with an increased risk of cardiovascular disease. In this context, the food industry has sought alternatives for the development of healthy lipid bases, with higher levels of unsaturated fatty adds, adapting to current legislation. The incorporation of structuring agents into liquid oils has proven to be a potential alternative for obtaining semiplastic lipid bases with reduced levels of saturated fatty adds. Thus, the objective of this study was to produce zero trans fat bases with lower saturated fatty acids levels. Palm oil (PO) was used as a zero trans-lipid base reference because of its technological functionality. Blends containing different proportions of high oleic sunflower oil (HOSO) and PO were prepared as follows: control 100: 0; 80:20; 60:40; 40:60; 20:80; and 100: 0 PO: HOSO (w/w%), respectively. Then, 3% of fully hydrogenated crambe oil (FHCO) and 3% sorbitan monostearate (SMS) were added to the blends as structuring agents, forming the structured (S) blends. The addition of HOSO to the PO decreased the saturated fatty acids by up to 30.6%, with consequent increase of unsaturated fatty acids, especially oleic add. The joint action of the SMS and the FCHO allowed for obtaining structured blends with plastic and spreadability characteristics, as well as modifications throughout the crystallization process of the original blends.

FOOD RESEARCH INTERNATIONAL 107, 61-72, 2018. DOI: 10.1016/j.foodres.2018.02.012

[P175-2018] "Study of dijet events with a large rapidity gap between the two leading jets in pp collisions at root s=7 TeV"

Sirunyan, A. M.; Tumasyan, A.; Adam, W.; **Chinellato, J. A.*; Tonelli Manganote, E. J.***; et al.
CMS Collaboration

Events with no charged particles produced between the two leading jets are studied in proton-proton collisions at root s = 7 TeV. The jets were required to have transverse momentum p(T) (jet) > 40 GeV and pseudorapidity 1.5 < vertical bar eta(jet)vertical bar < 4.7, and to have values of eta(jet) with opposite signs. The data used for this study were collected with the CMSdetector during low-luminosity running at the LHC, and correspond to an integrated luminosity of 8 pb(-1). Events with no charged particles with p(T) > 0.2GeV in the interval -1 < eta < 1 between the jets are observed in excess of calculations that assume no color-singlet exchange. The fraction of events with such a rapidity gap, amounting to 0.5-1% of the selected dijet sample, is measured as a function of the pT of the second-leading jet and of the rapidity separation between the jets. The data are compared to previous measurements at the Tevatron, and to perturbative quantum chromodynamics calculations based on the Balitsky-Fadin-Kuraev-Lipatov evolution equations, including different models of the non-perturbative gap survival probability.

EUROPEAN PHYSICAL JOURNAL C 78[3], 242, 2018. DOI: 10.1140/epjc/s10052-018-5691-6

[P176-2018] "Study of nitrogen ion doping of titanium dioxide films"

Ramos, R.*; Scoca, D.*; Merlo, R. B.*; Marques, F. C.*; Alvarez, F.*; Zagonel, L. F.*

This study reports on the properties of nitrogen doped titanium dioxide (TiO2) thin films considering the application as a transparent conducting oxide (TCO). Sets of thin films were prepared by sputtering a titanium target under oxygen atmosphere on a quartz substrate at 400 or 500 degrees C. Films were then doped at the same temperature by 150 eV nitrogen ions. The films were prepared in Anatase phase which was maintained after doping. Up to 30 at% nitrogen concentration was obtained at the surface, as determined by in situ X-ray photoelectron spectroscopy (XPS). Such high nitrogen concentration at the surface lead to nitrogen diffusion into the bulk which reached about 25 nm. Hall measurements indicate that average carrier density reached over 10(19) cm(-3) with mobility in the range of 0.1-1 cm(2) V-1 s(-1). Resistivity about 3 . 10(-1) Omega cm could be obtained with 85% light transmission at 550 nm. These results indicate that low energy implantation is an effective technique for TiO2 doping that allows an accurate control of the doping process independently from the TiO2 preparation. Moreover, this doping route seems promising to attain high doping levels without significantly affecting the film structure. Such approach could be relevant for preparation of N:TiO2 transparent conducting electrodes (TCE).

APPLIED SURFACE SCIENCE 443, 619-627, 2018. DOI: 10.1016/j.apsusc.2018.02.259

[P177-2018] "Suppression of Excited gamma States Relative to the Ground State in Pb-Pb Collisions at root s(NN)=5.02 TeV"

Sirunyan, A. M.; Tumasyan, A.; Adam, W.; **Chinellato, J. A.*; Tonelli Manganote, E. J.***; et al.
CMS Collaboration

The relative yields of gamma mesons produced in pp and Pb-Pb collisions at root s(NN) = 5.02 TeV and reconstructed via the dimuon decay channel are measured using data collected by the CMS experiment. Double ratios are formed by comparing the yields of the excited states, gamma(2S) and gamma(3S), to the ground state, gamma(1S), in both Pb-Pb and pp collisions at the same center-of-mass energy. The double ratios, [gamma(nS)/gamma(1S)](Pb-Pb)/[gamma(nS)/gamma(1S)](PP), are measured to be 0.308 +/- 0.055(stat) +/- 0.019(syst) for the gamma(2S) and less than 0.26 at 95% confidence level for the gamma(3S). No significant gamma(3S) signal is found in the Pb-Pb data. The double ratios are studied as a function of collision centrality, as well as gamma transverse momentum and rapidity. No significant dependencies are observed.

PHYSICAL REVIEW LETTERS 120[14], 142301, 2018. DOI: 10.1103/PhysRevLett.120.142301

[P178-2018] "The 2015 Summer Solstice Storm: One of the Major Geomagnetic Storms of Solar Cycle 24 Observed at Ground Level"

Augusto, C. R. A.; Navia, C. E.; de Oliveira, M. N.; Nepomuceno, A. A.; Raulin, J. P.; Tueros, E.; de Mendonca, R. R. S.; **Fauth, A. C.*; Vieira de Souza, H.***; Kopenkin, V.; Sinzi, T.

We report on the 22 - 23 June 2015 geomagnetic storm that occurred at the summer solstice. There have been fewer intense geomagnetic storms during the current solar cycle, Solar Cycle 24, than in the previous cycle. This situation changed after mid-June 2015, when one of the largest solar active regions (AR 12371) of Solar Cycle 24 that was located close to the central meridian,

produced several coronal mass ejections (CMEs) associated with M-class flares. The impact of these CMEs on the Earth's magnetosphere resulted in a moderate to severe G4-class geomagnetic storm on 22 - 23 June 2015 and a G2 (moderate) geomagnetic storm on 24 June. The G4 solstice storm was the second largest (so far) geomagnetic storm of Cycle 24. We highlight the ground-level observations made with the New-Tupi, Muonca, and the CARPET El Leoncito cosmic-ray detectors that are located within the South Atlantic Anomaly (SAA) region. These observations are studied in correlation with data obtained by space-borne detectors (ACE, GOES, SDO, and SOHO) and other ground-based experiments. The CME designations are taken from the Computer Aided CME Tracking (CACTus) automated catalog. As expected, Forbush decreases (FD) associated with the passing CMEs were recorded by these detectors. We note a peculiar feature linked to a severe geomagnetic storm event. The 21 June 2015 CME 0091 (CACTus CME catalog number) was likely associated with the 22 June summer solstice FD event. The angular width of CME 0091 was very narrow and measured degrees seen from Earth. In most cases, only CME halos and partial halos lead to severe geomagnetic storms. We perform a cross-check analysis of the FD events detected during the rise phase of Solar Cycle 24, the geomagnetic parameters, and the CACTus CME catalog. Our study suggests that narrow angular--width CMEs that erupt in a westward direction from the Sun--Earth line can lead to moderate and severe geomagnetic storms. We also report on the strong solar proton radiation storm that began on 21 June. We did not find a signal from this SEP at ground level. The details of these observations are presented.

SOLAR PHYSICS 293[5], 84, 2018. DOI: 10.1007/s11207-018-1303-8

[P179-2018] "The calculated low-energy side of the luminescence spectrum in zinc selenide"

Rodrigues, C. G.; **Luzzi, R.***

In this paper we consider electron-hole recombination in wide gap semiconductor ZnSe (Zinc Selenide) under electric fields. The calculated low energy side of the luminescence spectrum displays the so-called Urbach's tail, which is characterized as resulting from the presence of side bands in the form of replicas of the main band, corresponding to recombination with accompanying emission of one, two, three, etc., LO-phonons. Through the numerical solution of associate quantum transport equations based on the Non Equilibrium Statistical Operator Method, the carrier drift velocity and the nonequilibrium temperatures of electrons and phonons were obtained and the dependence on the electric field strength was determined. The influence of the applied electric field on the luminescence spectrum is evidenced. Our results for electric fields intensities of 5-25 kV/cm points to 15.7-19.7 meV Urbach tail widths in ZnSe.

JOURNAL OF LUMINESCENCE 199, 450-453, 2018. DOI: 10.1016/j.jlumin.2018.03.091

[P180-2018] "The Dark Energy Survey Image Processing Pipeline"

Morganson, E.; Gruendl, R. A.; Menanteau, F.; **Sobreira, F.***; et al.
DES Collaboration

The Dark Energy Survey (DES) is a five-year optical imaging campaign with the goal of understanding the origin of cosmic acceleration. DES performs a similar to 5000 deg(2) survey of the southern sky in five optical bands (g, r, i, z, Y) to a depth of similar to 24th magnitude. Contemporaneously, DES performs a deep, time-domain survey in four optical bands (g, r, i, z) over similar to 27 deg(2). DES exposures are processed nightly with an evolving data reduction pipeline and evaluated for image quality to determine if they need to be retaken. Difference imaging and transient source detection are also performed in the time domain component nightly. On a bi--annual basis, DES exposures are reprocessed with a refined pipeline and coadded to maximize imaging depth. Here we describe the DES image processing pipeline in support of DES science, as a reference for users of archival DES data, and as a guide for future astronomical surveys.

PUBLICATIONS OF THE ASTRONOMICAL SOCIETY OF THE PACIFIC 130[989], 074501, 2018. DOI: 10.1088/1538-3873/aab4ef

[P181-2018] "The free fall of an apple: conceptual subtleties and implications for physics teaching"

Assis, A. K. T.*; Karam, R. A. S.

The study of free fall is thoroughly present in physics teaching at all levels. From the point of view of Newtonian dynamics it appears to be extremely simple, as it consists of a two-body problem with a constant force generating a constant acceleration. However, there are several important conceptual subtleties and hidden assumptions involved in this problem, which are rarely discussed in educational settings. In this work we present some of these subtleties and argue that explicitly addressing them has significant pedagogical benefits.

EUROPEAN JOURNAL OF PHYSICS 39[3], 035003, 2018. DOI: 10.1088/1361-6404/aaa91d

[P182-2018] "The X-ARAPUCA: an improvement of the ARAPUCA device"

Machado, A. A.; **Segreto, E.*; Warner, D.; Fauth, A.*; Gelli, B.*; Maximo, R.*; Pissolatti, A.***; Paulucci, L.; Marinho, F.

The ARAPUCA is a novel technology for the detection of liquid argon scintillation light, which has been proposed for the far detector of the Deep Underground Neutrino Experiment. The X-ARAPUCA is an improvement to the original ARAPUCA design, retaining the original ARAPUCA concept of photon trapping inside a highly reflective box while using a wavelength shifting slab inside the box to increase the probability of collecting trapped photons onto a silicon photomultiplier array. The X-ARAPUCA concept is presented and its performances are compared to those of a standard ARAPUCA by means of analytical calculations and Monte Carlo simulations.

JOURNAL OF INSTRUMENTATION 13, C04026, 2018. DOI: 10.1088/1748-0221/13/04/C04026

[P183-2018] "Three-Dimensional Superlattice of PbS Quantum Dots in Flakes"

Ermakov, V. A.*; da Silva, J. M. C.*; Bonato, L. G.; Mogili, N. V. V.; Montoro, F. E.; **Iikawa, F.***; Nogueira, A. F.; **Cesar, C. L.*; Jimenez-Villar, E.*; Marques, F. C.***

In the last two decades, many experiments were conducted in self-organization of nanocrystals into two- and three--dimensional (3D) superlattices and the superlattices were synthesized and characterized by different techniques, revealing their unusual properties. Among all characterization techniques, X-ray diffraction (XRD) is the one that has allowed the confirmation of the 3D superlattice formation due to the presence of sharp and intense diffraction peaks. In this work, we study self-organized superlattices of quantum dots of PbS prepared by dropping a monodispersed colloidal solution on a glass substrate at different temperatures.

We showed that the intensity of the low-angle XRD peaks depends strongly on the drying time (substrate temperature). We claim that the peaks are originated from the 3D superlattice. Scanning electron microscopy images show that this 3D superlattice (PbS quantum dots) is formed in flake's shape, parallel to the substrate surface and randomly oriented in the perpendicular planes.

ACS OMEGA 3[2], 2027-2032, 2018. DOI: 10.1021/acsomega.7b01791

[P184-2018] "Titanium-Carbide Formation at Defective Curved Graphene-Titanium Interfaces"

Fonseca, A. F.*; Liang, T.; Zhang, D. F.; Choudhary, K.; Phillpot, S. R.; Sinnott, S. B.

Physical and chemical properties of graphene-metal interfaces have been largely examined with the objective of producing nanostructured carbon-based electronic devices. Although electronic properties are key to such devices, appropriate structural, thermal and mechanical properties are important for device performance as well. One of the most studied is the graphene-titanium (G-Ti) interface. Titanium is a low density, high strength versatile metal that can form alloys with desirable properties for applications ranging from aerospace to medicine. Small clusters and thin films of titanium deposited on graphene have also been examined. However, while some experiments show that thin films of titanium on graphene can be removed without damaging graphene hexagonal structure, others reported the formation of titanium-carbide (TiC) at G-Ti interfaces. In a previous work [ACS Appl. Mater. Interfaces, 2017, 9 (38), pp 33288-33297], we have shown that pristine G-Ti interfaces are resilient to large thermal fluctuations even when G-Ti structures lie on curved or kinked substrates. Here, using classical molecular dynamics with the third-generation Charge Optimized Many Body (COMB3) potential, we show that di-interstitial defective G-Ti structures on a copper substrate with a relatively large curvature kink, present signs of TiC formation. This result might help explain the different experimental results mentioned above.

MRS ADVANCES 3[8-9], 454-459, 2018. DOI: 10.1557/adv.2018.115

[P185-2018] "Tuning dipolar magnetic interactions by controlling individual silica coating of iron oxide nanoparticles"

Rivas Rojas, P. C.; Tancredi, P.; **Moscoso Londono, O.*; Knobel, M.***; Socolovsky, L. M.

Single and fixed size core, core-shell nanoparticles of iron oxides coated with a silica layer of tunable thickness were prepared by chemical routes, aiming to generate a frame of study of magnetic nanoparticles with controlled dipolar interactions. The batch of iron oxides nanoparticles of 4.5 nm radii, were employed as cores for all the coated samples. The latter was obtained via thermal decomposition of organic precursors, resulting on nanoparticles covered with an organic layer that was subsequently used to promote the ligand exchange in the inverse microemulsion process, employed to coat each nanoparticle with silica. The amount of precursor and times of reaction was varied to obtain different silica shell thicknesses, ranging from 0.5 nm to 19 nm. The formation of the desired structures was corroborated by TEM and SAXS measurements, the core single-phase spinel structure was confirmed by XRD, and superparamagnetic features with gradual change related to dipolar interaction effects were obtained by the study of the applied field and temperature dependence of the magnetization. To illustrate that dipolar interactions are consistently controlled, the main magnetic properties are presented and analyzed as a function of center to center minimum distance between the magnetic cores.

JOURNAL OF MAGNETISM AND MAGNETIC MATERIALS 451, 688-696, 2018. DOI: 10.1016/j.jmmm.2017.11.099

[P186-2018] "UV-luminous, star-forming hosts of z similar to 2 reddened quasars in the Dark Energy Survey"

Wethers, C. F.; Banerji, M.; Hewett, P. C.; **Sobreira, F.***; et al.

We present the first rest-frame UV population study of 17 heavily reddened, high-luminosity [E(B - V)(QSO) greater than or similar to 0.5; L-bol > 10(46) erg s(-1)] broad-line quasars at 1.5 < z < 2.7. We combine the first year of deep, optical, ground-based observations from the Dark Energy Survey (DES) with the near-infrared VISTA Hemisphere Survey and UKIDSS Large Area Survey data, from which the reddened quasars were initially identified. We demonstrate that the significant dust reddening towards the quasar in our sample allows host galaxy emission to be detected at the rest-frame UV wavelengths probed by the DES photometry. By exploiting this reddening effect, we disentangle the quasar emission from that of the host galaxy via spectral energy distribution fitting. We find evidence for a relatively unobscured, star-forming host galaxy in at least 10 quasars, with a further three quasars exhibiting emission consistent with either star formation or scattered light. From the rest-frame UV emission, we derive instantaneous, dust-corrected star formation rates (SFRs) in the range 25 < SFRUV < 365 M-circle dot yr(-1), with an average SFRUV = 130 + 95 M-circle dot yr(-1). We find a broad correlation between SFRUV and the bolometric quasar luminosity. Overall, our results show evidence for coeval star formation and black hole accretion occurring in luminous, reddened quasars at the peak epoch of galaxy formation.

MONTHLY NOTICES OF THE ROYAL ASTRONOMICAL SOCIETY 475[3], 3682-3699, 2018. DOI: 10.1093/mnras/stx3332

[P187-2018] "Versatile silicon-waveguide supercontinuum for coherent mid-infrared spectroscopy"

Nader, N.; Maser, D. L.; **Cruz, F. C.***; Kowligy, A.; Timmers, H.; Chiles, J.; Fredrick, C.; Westly, D. A.; Nam, S.; Mirin, R. P.; Shainline, J. M.; Diddams, S.

Laser frequency combs, with their unique combination of precisely defined spectral lines and broad bandwidth, are a powerful tool for basic and applied spectroscopy. Here, we report offset-free, mid-infrared frequency combs and dual-comb spectroscopy through supercontinuum generation in silicon-on--sapphire waveguides. We leverage robust fabrication and geometrical dispersion engineering of nanophotonic waveguides for multi-band, coherent frequency combs spanning 70 THz in the mid-infrared (2.5 mu m-6.2 mu m). Precise waveguide fabrication provides significant spectral broadening with engineered spectra targeted at specific mid-infrared bands. We characterize the relative-intensity-noise of different bands and show that the measured levels do not pose any limitation for spectroscopy applications. Additionally, we use the fabricated photonic devices to demonstrate dual-comb spectroscopy of a carbonyl sulfide gas sample at 5 mu m. Thiswork forms the technological basis for applications such as point sensors for fundamental spectroscopy, atmospheric chemistry, trace and hazardous gas detection, and biological microscopy.

APL PHOTONICS 3[3], 036102, 20108. DOI: 10.1063/1.5006914

[P188-2018] "Virtually imprinted polymers (VIPs): understanding molecularly templated materials via molecular dynamics simulations"

Zink, S.; **Moura, F. A.***; Autreto, P. A. D.; **Galvao, D. S.***; Mizaikoff, B.

Molecularly imprinted polymers are advanced recognition materials selectively rebinding a target molecule present during the synthesis of the polymer matrix. It is commonly understood that the templating process is based on embedding the complex formed between a template and functional monomers into a co-polymer matrix. This happens by a polymerization of the complex with a crosslinker while maintaining their spatial arrangement forming a molecular imprint. Template removal then leads to synthetic recognition sites ready to selectively rebind their targets, which are complementary in functionality, size and shape to the target. In this study, an innovative theoretical concept using fully atomistic molecular dynamics simulations for modeling molecular templating processes is introduced yielding virtually imprinted polymers (VIPs). VIPs created for the template 17-b-estradiol and applied in modeled chromatography experiments demonstrated selectivity for their template. This evidenced the creation of virtual imprints as a result of a templated synthesis protocol, which represents a theoretical confirmation of the governing imprinting theory.

PHYSICAL CHEMISTRY CHEMICAL PHYSICS 20[19], 13145-13152, 2018. DOI: 10.1039/c7cp08284c

[P189-2018] "Water/Alcohol Separation in Graphene Oxide Membranes: Insights from Molecular Dynamics and Monte Carlo Simulations"

Borges, D. D.*; Woellner, C. F.*; Autreto, P. A. S.; **Galvao, D. S.***

Graphene-based membranes have been investigated as promising candidates for water filtration and gas separation applications. Experimental evidences have shown that graphene oxide can be impermeable to liquids, vapors and gases, while allowing a fast permeation of water molecules. This phenomenon has been attributed to the formation of a network of nano capillaries that allow nearly frictionless water flow while blocking other molecules by steric hindrance effects. It is supposed that water molecules are transported through the percolated two-dimensional channels formed between graphene-based sheets. Although these channels allow fast water permeation in such materials, the flow rates are strongly dependent on how the membranes are fabricated. Also, some fundamental issues regarding the nanoscale mechanisms of water permeation are still not fully understood and their interpretation remains controversial. In this work, we have investigated the dynamics of water permeation through pristine graphene and graphene oxide model membranes that have strong impact on water/alcohol separation. We have carried out fully atomistic classical molecular dynamics simulations of systems composed of multiple layered graphene-based sheets into contact with a pure water reservoir under controlled thermodynamics conditions (e.g., by varying temperature and pressure values). We have systematically analysed how the transport dynamics of the confined nanofluids depend on the interlayer distances and the role of the oxide functional groups. Our results show the water flux is much more effective for graphene than for graphene oxide membranes. These results can be attributed to the H-bonds formation between oxide functional groups and water, which traps the water molecules and precludes ultrafast water transport through the nanochannels.

MRS ADVANCES 3[1-2], 109-114, 2018. DOI: 10.1557/adv.2018.192

Meeting Abstract

[Me001-2018] "Monte Carlo Evaluation of Radionuclides for Early Brain Metastases Targeting"

Falzone, N.; Ackerman, N. L.; **de la Fuente Rosales, L.*; Bernal, M. A.***; Peeters, S. G. J. A.; Soto, M. S.; Sibson, N. R.; Vallis, K. A.

INTERNAL MEDICINE JOURNAL 48[SI], 9-10 Sup. 3, O-011, 2018.

Correções

[Co003-2018] "Experimental setup for measuring the barocaloric effect in polymers: Application to natural rubber (vol 88, 046103, 2017)"

Bom, N. M.; Usuda, E. O.; Guimaraes, G. M.; **Coelho, A. A.***; Carvalho, A. M. G.

REVIEW OF SCIENTIFIC INSTRUMENTS 89[3], 039901, 2018. DOI: 10.1063/1.5026289

***Autores da comunidade IFGW**
Fonte: Web of Science on-line (WOS)

Defesas de Dissertações do IFGW

[D008-2018] "Otimização da qualidade da imagem e dose em radiologia pediátrica usando simulação Monte Carlo e Métodos Experimentais"
Aluno: Hítalo Rodrigues Mendes
Orientador: Profa. Dra. Alessandra Tomal
Data: 21/06/2018

[D009-2018] "Oscilações acústicas bariônicas"
Aluno: Anderson Luiz Brandão de Souza
Orientador: Prof. Dr. Pedro Cunha de Holanda
Data: 29/06/2018

Defesas de Teses do IFGW

[T011-2018] "Estudo do Dano Direto e Indireto Induzido ao DNA pela Radiação Ionizante Usando o Método de Monte Carlo"
Aluno: Liset De la Fuente Rosales
Orientador: Prof. Dr. Mario Antonio Bernal Rodriguez
Data: 28/06/2018

[T012-2018] "Controle, preservação e transferência de emaranhamento quântico em sistemas abertos a altas temperaturas"
Aluno: Julio Cesar González Henao
Orientador: Prof. Dr. José Antonio Roversi
Data: 02/07/2018

Fonte: Portal IFGW/Pós-graduação - Agenda de Colóquios, Defesas e Seminários.
Disponível em: http://portal.ifi.unicamp.br/pos-graduacao

Fique por dentro!
Cadastre-se como leitor, e receba os avisos da publicação de novos números por e-mail.

<http://abstracta.ifi.unicamp.br>

Abstracta

Instituto de Física
Diretor: Prof. Dr. Pascoal José Giglio Pagliuso
Diretora Associada: Profa. Dra. Mônica Alonso Cotta
Universidade Estadual de Campinas - UNICAMP
Cidade Universitária Zeferino Vaz
13083-859 - Campinas - SP - Brasil
e-mail: secdir@ifi.unicamp.br
Fone: +55 19 3521-5300

Publicação

Biblioteca do Instituto de Física Gleb Wataghin
http://portal.ifi.unicamp.br/biblioteca

Diretora Técnica: Sandra Maria Carlos Cartaxo
Coordenadora da Comissão de Biblioteca: Profa. Dra. Arlene Cristina Aguilar

Elaboração:
Maria Graciele Trevisan (Bibliotecária)
contato: infobif@ifi.unicamp.br